Monthly Notices
of the
ROYAL ASTRONOMICAL SOCIETY

MNRAS **488,** 18–36 (2019)
Advance Access publication 2019 June 13

doi:10.1093/mnras/stz1633

Six new rapidly oscillating Ap stars in the *Kepler* long-cadence data using super-Nyquist asteroseismology

Daniel R. Hey [1,2]★ Daniel L. Holdsworth [3] Timothy R. Bedding [1,2] Simon J. Murphy,[1,2] Margarida S. Cunha [4] Donald W. Kurtz [3] Daniel Huber [5] Benjamin Fulton [6] and Andrew W. Howard [7]

[1] *School of Physics, Sydney Institute for Astronomy (SIfA), The University of Sydney, NSW 2006, Australia*
[2] *Stellar Astrophysics Centre, Aarhus University, DK-8000 Aarhus C, Denmark*
[3] *Jeremiah Horrocks Institute, University of Central Lancashire, Preston PR1 2HE, UK*
[4] *Instituto de Astrofísica e Ciências do Espaço, Universidade do Porto, CAUP, Rua das Estrelas, P-4150-762 Porto, Portugal*
[5] *Institute for Astronomy, University of Hawai'i, 2680 Woodlawn Drive, Honolulu, HI 96822, USA*
[6] *NASA Exoplanet Science Institute/Caltech-IPAC, Pasadena, CA 91125, USA*
[7] *California Institute of Technology, Pasadena, CA 91125, USA*

Accepted 2019 June 10. Received 2019 June 8; in original form 2019 May 9

ABSTRACT

We perform a search for rapidly oscillating Ap stars in the *Kepler* long-cadence data, where true oscillations above the Nyquist limit of 283.21 μHz can be reliably distinguished from aliases as a consequence of the barycentric time corrections applied to the *Kepler* data. We find evidence for rapid oscillations in six stars: KIC 6631188, KIC 7018170, KIC 10685175, KIC 11031749, KIC 11296437, and KIC 11409673, and identify each star as chemically peculiar through either pre-existing classifications or spectroscopic measurements. For each star, we identify the principal pulsation mode, and are able to observe several additional pulsation modes in KIC 7018170. We find that KIC 7018170 and KIC 11409673 both oscillate above their theoretical acoustic cut-off frequency, whilst KIC 11031749 oscillates at the cut-off frequency within uncertainty. All but KIC 11031749 exhibit strong amplitude modulation consistent with the oblique pulsator model, confirming their mode geometry and periods of rotation.

Key words: asteroseismology – techniques: photometric – stars: chemically peculiar – stars: oscillations.

1 INTRODUCTION

Since their discovery by Kurtz (1978, 1982), only 70 rapidly oscillating Ap (roAp) stars have been found (Smalley et al. 2015; Joshi et al. 2016; Balona, Holdsworth & Cunha 2019; Cunha et al. 2019). Progress in understanding their pulsation mechanism, abundance, and the origin of their magnetic fields has been hindered by the relatively small number of known roAp stars. A key difficulty in their detection lies in the rapid oscillations themselves, requiring dedicated observations at a short enough cadence to properly sample the oscillations. In this paper, we show that the *Kepler* long-cadence (LC) data can be used to detect roAp stars, despite their pulsation frequencies being greater than the Nyquist frequency of the data.

As a class, the chemically peculiar A type (Ap) stars exhibit enhanced features of rare Earth elements, such as Sr, Cr, and Eu, in their spectra (Morgan 1933). This enhancement is the result of a stable magnetic field of the order of a few to tens of kG (Mathys 2017), which typically allows for the formation of abundance 'spots' on the surface, concentrated at the magnetic poles (Ryabchikova et al. 2007). In most, but not all Ap stars, photometric and spectral variability over the rotation cycle can be observed (Abt & Morrell 1995). Such characteristic spot-based modulation manifests as a low-frequency modulation of the light curve which is readily identified, allowing for the rotation period to be measured (e.g. Drury et al. 2017).

The roAp stars are a rare subclass of the Ap stars that exhibit rapid brightness and radial velocity variations with periods between 5 and 24 min and amplitudes up to 0.018 mag in Johnson *B* (Kurtz 2000; Kochukhov 2009). They oscillate in high overtone, low-degree pressure (p) modes (Saio 2005). The excitation of high-overtone p modes, as opposed to the low overtones of other pulsators in the classical instability strip is suspected to be a consequence of the strong magnetic field – of the order of a few to tens of kG – which suppresses the convective envelope at the magnetic poles and increases the efficiency of the opacity mechanism in the region of hydrogen ionization (Balmforth et al. 2001; Cunha 2002). Based on this, a theoretical instability strip for the roAp stars has been

★ E-mail: danielhey@outlook.com

published by Cunha (2002). However, discrepancies between the observed and theoretical red and blue edges have been noted, with several roAp stars identified to be cooler than the theoretical red edge.

A further challenge to theoretical models of pulsations in magnetic stars are oscillations above the so-called acoustic cut-off frequency (Saio 2013; Holdsworth et al. 2018b). In non-magnetic stars, oscillations above this frequency are not expected. However, in roAp stars the strong magnetic field guarantees that part of the wave energy is kept inside the star in every pulsation cycle, for arbitrarily large frequencies (Sousa & Cunha 2008). For that reason, no theoretical limit exists to the frequency of the modes. Nevertheless, for a mode to be observed, it has to be excited. Models show that the opacity mechanism is capable of exciting modes of frequency close to, but below, the acoustic cut-off frequency. The excitation mechanism for the oscillations above the acoustic cut-off is thought to be turbulent pressure in the envelope regions where convection is no longer suppressed (Cunha et al. 2013).

The magnetic axis of roAp stars is closely aligned with the pulsation axis, with both being inclined to the rotation axis. Observation of this phenomenon led to the development (Kurtz 1982) and later refinement (Dziembowski & Goode 1985; Shibahashi & Saio 1985a,b; Shibahashi & Takata 1993; Takata & Shibahashi 1994, 1995; Bigot & Kurtz 2011) of the oblique pulsator model. The roAp stars present a unique testbed for models of magneto-acoustic interactions in stars, and have been widely sought with both ground and space-based photometry.

The launch of the *Kepler* Space Telescope allowed for the detection of oscillations well below the amplitude threshold for ground-based observations, even for stars fainter than 13 mag. The vast majority of stars observed by *Kepler* were recorded in LC mode, with exposures integrated over 29.43 min. A further allocation of 512 stars at any given time were observed in the short-cadence (SC) mode, with an integration time of 58.85 s. These two modes correspond to Nyquist limits of 283.21 and 8496.18 μHz, respectively (Borucki et al. 2010). In its nominal mission, *Kepler* continuously observed around 150 000 stars in LC mode for 4 yr.

The *Kepler* SC data have been used to discover several roAp stars (Kurtz et al. 2011; Balona et al. 2011a, 2013; Smalley et al. 2015), and to detect pulsation in previously known roAp stars with the extended K2 mission (Holdsworth et al. 2016, 2018a). Until now, only SC data have been used for identification of new roAp stars in the *Kepler* field. However, with the limited availability of SC observation slots, a wide search for rapid oscillators has not been feasible. Although ground-based photometric data have been used to search for roAp stars (e.g. Martinez, Kurtz & Kauffmann 1991; Joshi 2005; Paunzen et al. 2012; Holdsworth et al. 2014a), most previous work in using *Kepler* to identify such stars has relied solely on SC observations of targets already known to be chemically peculiar. The number of targets in the *Kepler* field that possess LC data far outweigh those with SC data, but they have been largely ignored in the search for new roAp stars.

The key difficulty in searching for rapid oscillations in the LC data is that each pulsation frequency in the Fourier spectrum is accompanied by many aliases, reflected around integer multiples of the sampling frequency. Despite this, it has previously been shown by Murphy, Shibahashi & Kurtz (2013) that the Nyquist ambiguity in the LC data can be resolved as a result of the barycentric corrections applied to *Kepler* time stamps, leading to a scenario where Nyquist aliases can be reliably distinguished from their true counterparts even if they are well above or below the nominal Nyquist limit. The barycentric corrections modulate the cadence of the photometric observations, so that all aliases above the Nyquist limit appear as multiplets split by the orbital frequency of the *Kepler* telescope (1/372.5 d, 0.03 μHz). Furthermore, the distribution of power in Fourier space ensures that in the absence of errors, the highest peak of a set of aliases will always be the true one. An example of distinguishing aliases is shown in Fig. 1 for the known roAp star KIC 10195926. The true pulsation is evident as the highest peak in the LC data, and is not split by the *Kepler* orbital frequency.

This technique, known as super-Nyquist asteroseismology, has previously been used with red giants and solar-like oscillators on a case-by-case basis (Chaplin et al. 2014; Mathur et al. 2016; Yu et al. 2016), as well as in combinations of LC data with ground-based observations for compact pulsators (Bell et al. 2017). Applications in the context of roAp stars have been limited only to frequency verification of SC or other data (Holdsworth et al. 2014b; Smalley et al. 2015). Our approach makes no assumption about the spectroscopic nature or previous identification of the target, except that its effective temperature lies in the observed range for roAp stars. We further note that super-Nyquist asteroseismology is applicable to the Transiting Exoplanet Survey Satellite (TESS; Ricker et al. 2014) and future space-based missions (Murphy 2015c; Shibahashi & Murphy 2018).

In this paper, we report six new roAp stars whose frequencies are identified solely from their LC data; KIC 6631188, KIC 7018170, KIC 10685175, KIC 11031749, KIC 11296437, and KIC 11409673. These are all found to be chemically peculiar A/F stars with enhanced Sr, Cr, and/or Eu lines.

2 OBSERVATIONAL DATA AND ANALYSIS

2.1 Target selection

We selected *Kepler* targets with effective temperatures between 6000 and 10 000 K according to the 'input' temperatures of Mathur et al. (2017). We significantly extended the cooler edge of our search since few roAp stars are known to lie close to the red edge of the instability strip. We used the *Kepler* LC light curves from Quarters 0 through 17, processed with the PDCSAP pipeline (Stumpe et al. 2014), yielding a total sample of 69 347 stars. We applied a custom-written pipeline to all of these stars that have LC photometry for at least four quarters. Nyquist aliases in stars with time-bases shorter than a full Kepler orbital period (4 quarters) have poorly defined multiplets and were discarded from the sample at run-time (see Murphy et al. 2013, for details).

In addition to the automated search, we manually inspected the light curves of the 53 known magnetic chemically peculiar (mCP) stars from the list of Hümmerich et al. (2018). These stars have pre-existing spectral classification, requiring only a super-Nyquist oscillation to be identified as a roAp star.

2.2 Pipeline

The pipeline was designed to identify all oscillations between 580 and 3500 μHz in the *Kepler* LC data, by first applying a high-pass filter to the light curve, removing both the long-period rotational modulation between 0 and 50 μHz and low-frequency instrumental artefacts. The high-pass filter reduced all power in this given range to noise level. The skewness of the amplitude spectrum values, as measured between 0 and 3500 μHz, was then used as a diagnostic for separating pulsators and non-pulsators, following Murphy et al. (2019). Stars with no detectable pulsations, either

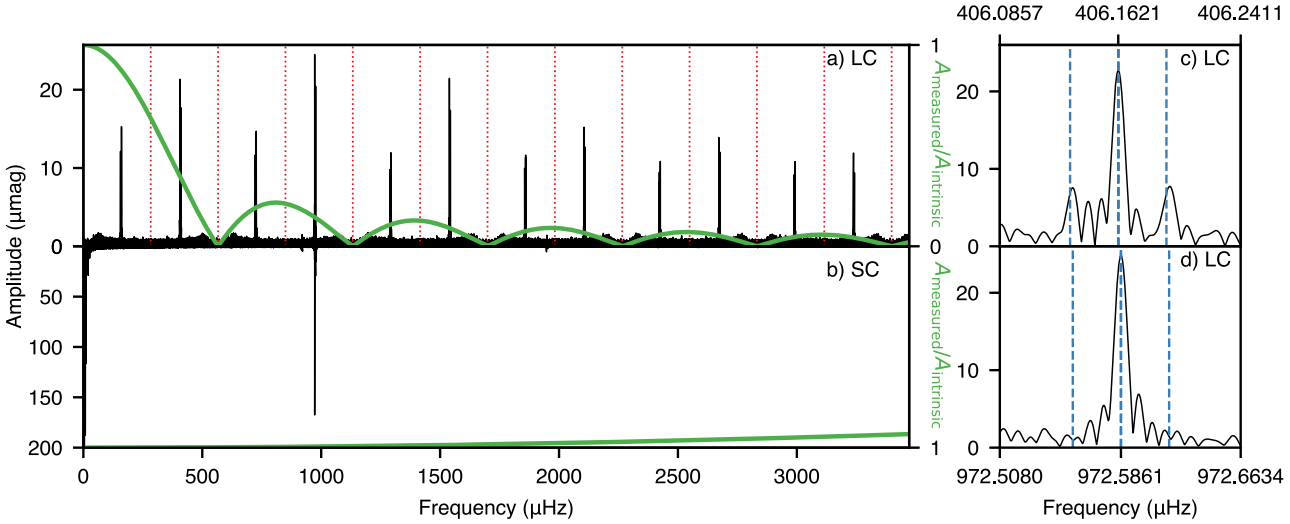

Figure 1. Amplitude spectra of the (a) long- and (b) short-cadence *Kepler* data of KIC 10195926, a previously known roAp star (Kurtz et al. 2011). The primary oscillation is detectable even though it lies far above the Nyquist frequency (shown in integer multiples of the Nyquist frequency as red dotted lines) for the LC data. The green curves show the ratio of measured to intrinsic amplitudes in the data, showing the effects of apodization. (c) shows the aliased signal at 406.2 μHz of the true oscillation at (d), 972.6 μHz, distinguishable by both the *Kepler* orbital separation frequency (dashed blue lines) and maximum amplitudes. The PYTHON code PYQUIST has been used to plot the apodization (Bell et al. 2017).

aliased or otherwise, tend to have a skewness lower than unity, and were removed from the sample.

After filtering out non-pulsators, each frequency above 700 μHz at a signal-to-noise ratio (SNR) greater than 5 was then checked automatically for sidelobes. These sidelobes are caused by the uneven sampling of *Kepler*'s data points once barycentric corrections to the time stamps have been made, as seen in Fig. 1. A simple peak-finding algorithm was used to determine the frequency of highest amplitude for each frequency in the set of aliases, which was further refined using a three-point parabolic interpolation to mitigate any potential frequency drift. The frequencies above an SNR of 5 were then deemed aliases if their sidelobes were separated by the *Kepler* orbital frequency for a tolerance of ±0.002 μHz. Frequencies that did not display evidence of Nyquist aliasing were then flagged for manual inspection.

The general process for the pipeline can be summarized as follows:

(i) High-pass filter the light curve and calculate the skewness of the amplitude spectrum between 0 and 3500 μHz; if skewness is less than unity, move to next star.

(ii) For each peak greater than 700 μHz with an SNR above 5, identify all sidelobes and determine whether they are separated by the *Kepler* orbital frequency.

(iii) If at least one peak is not an alias, flag the star for manual inspection.

2.3 Apodization

The high-pass filter was designed to remove all signals between 0 and 50 μHz. This had the additional effect of removing the reflected signals at integer multiples of the sampling frequency, regardless of whether they are aliased or genuine. As a result, the pipeline presented here cannot reliably identify oscillations close to integer multiples of the sampling frequency ($2\nu_{\rm Nyq}$).

However, we note that if any of these stars are indeed oscillating in these regions, or even above the Nyquist frequency, the measured amplitude will be highly diminished as a result of the non-zero duration of *Kepler* integration times, a phenomenon referred to as apodization (Murphy 2015a; Hekker & Christensen-Dalsgaard 2017) or phase smearing (Bell et al. 2017). The amplitudes measured from the data ($A_{\rm measured}$) are smaller than their intrinsic amplitudes in the *Kepler* filter by a factor of η,

$$\eta = \frac{A_{\rm measured}}{A_{\rm intrinsic}} = \mathrm{sinc}\left[\frac{\pi\nu}{2\nu_{\rm Nyq}}\right], \quad (1)$$

where ν and $\nu_{\rm Nyq}$ are the observed and Nyquist frequencies, respectively. This equation shows that frequencies lying near integer multiples of the sampling frequency are almost undetectable in *Kepler* and other photometric campaigns. The factor η is shown as the green curves in Fig. 1. For the results in Section 3, both measured and intrinsic amplitudes are provided.

3 RESULTS

Each star found to have non-alias high-frequency pulsations by the pipeline was manually inspected. Of the flagged candidates, four were previously identified roAp stars in the *Kepler* field, KIC 10195926 (Kurtz et al. 2011), KIC 10483436 (Balona et al. 2011b), KIC 7582608 (Holdsworth et al. 2014b), and KIC 4768731 (Smalley et al. 2015). The fifth previously known *Kepler* roAp star KIC 8677585 (Balona et al. 2013), was not identified by the pipeline, due to the primary frequency of 1659.79 μHz falling just within range of the filtered region. We further identified one more high-frequency oscillator during manual inspection of the 53 stars in the mCP sample of Hümmerich et al. (2018).

For all six newly identified stars, we calculated an amplitude spectrum in the frequency range around the detected pulsation, following the method of Kurtz (1985). The frequencies were then optimized by non-linear least squares. The S/N of the spectrum was calculated for the entire light curve by means of a box kernel convolution of frequency width 23.15 μHz (2 d^{-1}), as implemented in the LIGHTKURVE PYTHON package (Vinícius et al. 2018).

Table 1. Properties of the six new roAp stars.

KIC	g mag	$T_{\rm eff}$ (K)	$\log L/L_\odot$	$M/M_\odot$
6631188	13.835	7700 ± 300	1.124 ± 0.034	1.83 ± 0.25
7018170	13.335	7000 ± 300	0.987 ± 0.026	1.69 ± 0.25
10685175	12.011	8000 ± 300	0.896 ± 0.022	1.65 ± 0.25
11031749	12.949	7000 ± 300	1.132 ± 0.041	1.78 ± 0.25
11296437	11.822	7000 ± 300	1.055 ± 0.018	1.73 ± 0.25
11409673	12.837	7500 ± 300	1.056 ± 0.031	1.75 ± 0.25

3.1 Stellar properties

The properties of the six new high-frequency oscillators examined in this work are provided in Table 1. Temperatures were obtained from LAMOST DR4 spectroscopy (Zhao et al. 2012). Since the temperatures of roAp stars are inherently difficult to measure as a result of their anomalous elemental distributions (Matthews, Kurtz & Martinez 1999), we inflated the low uncertainties in the LAMOST catalogue ($\sim$40 K) to a fixed 300 K. For the one star with an unusable spectrum in LAMOST, KIC 6631188, we took the temperature from the stellar properties catalogue of Mathur et al. (2017). We derived apparent magnitudes in the SDSS g band by re-calibrating the KIC g and r bands following equation (1) of Pinsonneault et al. (2012). Distances were obtained from the *Gaia* DR2 parallaxes using the normalized posterior distribution and adopted length-scale model of Bailer-Jones et al. (2018). This produced a distribution of distances for each star, from which Monte Carlo draws could be sampled. Unlike Bailer-Jones et al. (2018), no parallax zero-point correction has been applied to our sample, since it has previously been shown by Murphy et al. (2019) to not be appropriate for *Kepler* A stars.

Standard treatment of bolometric corrections (e.g. Torres 2010) is unreliable for Ap stars, due to their anomalous flux distributions. Working in SDSS g minimizes the bolometric correction, since the wavelength range is close to the peak of the spectral energy distribution of Ap stars. We obtained g-band bolometric corrections using the ISOCLASSIFY package (Huber et al. 2017), which interpolates over the MESA Isochrones & Stellar Tracks (MIST) tables (Dotter 2016) using stellar metallicities, effective temperatures, and surface gravities obtained from Mathur et al. (2017). Extinction corrections of Green et al. (2018) as queried through the DUSTMAPS PYTHON package (Green 2018), were applied to the sample. The corrections were re-scaled to SDSS g following table A1 of Sanders & Das (2018). To calculate luminosities, we followed the methodology of Murphy et al. (2019), using a Monte Carlo simulation to obtain uncertainties. Masses were obtained via an interpolation over stellar tracks, and are discussed in more detail in Section 5.3.

4 DISCUSSION OF INDIVIDUAL STARS

4.1 KIC 6631188

KIC 6631188 has previously been identified as a rotational variable with a period of 5.029 d (Reinhold, Reiners & Basri 2013), or 2.514 d (Reinhold & Gizon 2015). The unfiltered light curve of KIC 6631188 shows a series of low-frequency harmonic signals beginning at multiples of 2.30 μHz (Fig. 2). Although the highest amplitude signal corresponds to a rotational period of 2.514 d, the true rotation period was confirmed by folding the light curve on the 2.30 μHz frequency, yielding a period of 5.03117 ± 0.00004 d. The folded light curve shows clear double-wave spot-based modulation, implying that both magnetic poles are observed.

After high-pass filtering the light curve, the primary pulsation frequency of 1493.52 μHz is observable in the super-Nyquist regime. We see evidence for rotational splitting through the detection of a quintuplet, indicating an $\ell = 2$ or distorted $\ell = 1$ mode. It seems likely that the star is a pure quadrupole pulsator, unless an $\ell = 1$ mode is hidden at an integer multiple of the sampling frequency – where its amplitude would be highly diminished as a result of apodization. It is also possible that other modes are of low intrinsic amplitude, making their detection in the super-Nyquist regime difficult. We can measure the rotational period of KIC 6631188 from the sidelobe splitting as 5.0312 ± 0.0003 d in good agreement with the low-frequency signal. We list the pulsation and rotational frequencies in Table 2.

We are able to provide further constraints on the geometry of the star by assuming that the rotational sidelobes are split from the central peak by exactly the rotation frequency of the star. We chose a zero-point in time such that the phases of the sidelobes were equal, and then applied a linear least-squares fit to the data. For a pure non-distorted mode, we expect the phases of all peaks in the multiplet to be the same. We find that the phases are not identical, implying moderate distortion of the mode (Table 3).

The oblique pulsator model can also be applied to obtain geometric constraints on the star's magnetic obliquity and inclination angles, β and i, respectively. The frequency quintuplet strongly suggests that the pulsation in KIC 6631188 is a quadrupole mode. We therefore consider the axisymmetric quadrupole case, where $\ell = 2$ and $m = 0$ and apply the relation of Kurtz (1990) for a non-distorted oblique quadrupole pulsation in the absence of limb darkening and spots:

$$\tan i \tan \beta = 4 \frac{A^{(2)}_{+2} + A^{(2)}_{-2}}{A^{(2)}_{+1} + A^{(2)}_{-1}}. \quad (2)$$

Here i is the rotational inclination angle, β is the angle of obliquity between the rotation and magnetic axes, and $A^{(1,2)}_{\pm 1,2}$ are the amplitudes of the first and second sidelobes of the quadrupole pulsation. Using the values of Table 3, we find that $\tan i \tan \beta = 7.4 \pm 0.7$, and provide a summary of values satisfying this relation in Fig. 3. Since $i + \beta \geq 90^\circ$, both pulsation poles should be visible in the light curve over the rotation cycle of the star, a result consistent with observations of the double-wave light curve with spots at the magnetic poles.

4.2 KIC 7018170

The low-frequency variability of KIC 7018170 exhibits no sign of rotational modulation, which is probably a result of the PDCSAP pipeline removing the long-period variability (Fig. 4). It is therefore unsurprising that KIC 7018170 has not been detected as an Ap star in the *Kepler* data – the automatic removal of low-frequency modulation causes it to appear as an ordinary non-peculiar star in the LC photometry.

The rotational signal is clearly present in the sidelobe splitting of the primary and secondary pulsation frequencies. The high-pass filtered light curve reveals the primary signal, ν_1, at 1945.30 μHz, with inspection of the amplitude spectrum revealing two more modes; ν_2 and ν_3, at frequencies of 1920.28 and 1970.32 μHz, respectively. All three of these modes are split by 0.16 μHz which we interpret as the rotational frequency. KIC 7018170 exhibits significant frequency variability during the second half of the data, which destroys the clean peaks of the triplets. To analyse them in detail, we analysed only the first half of the data where

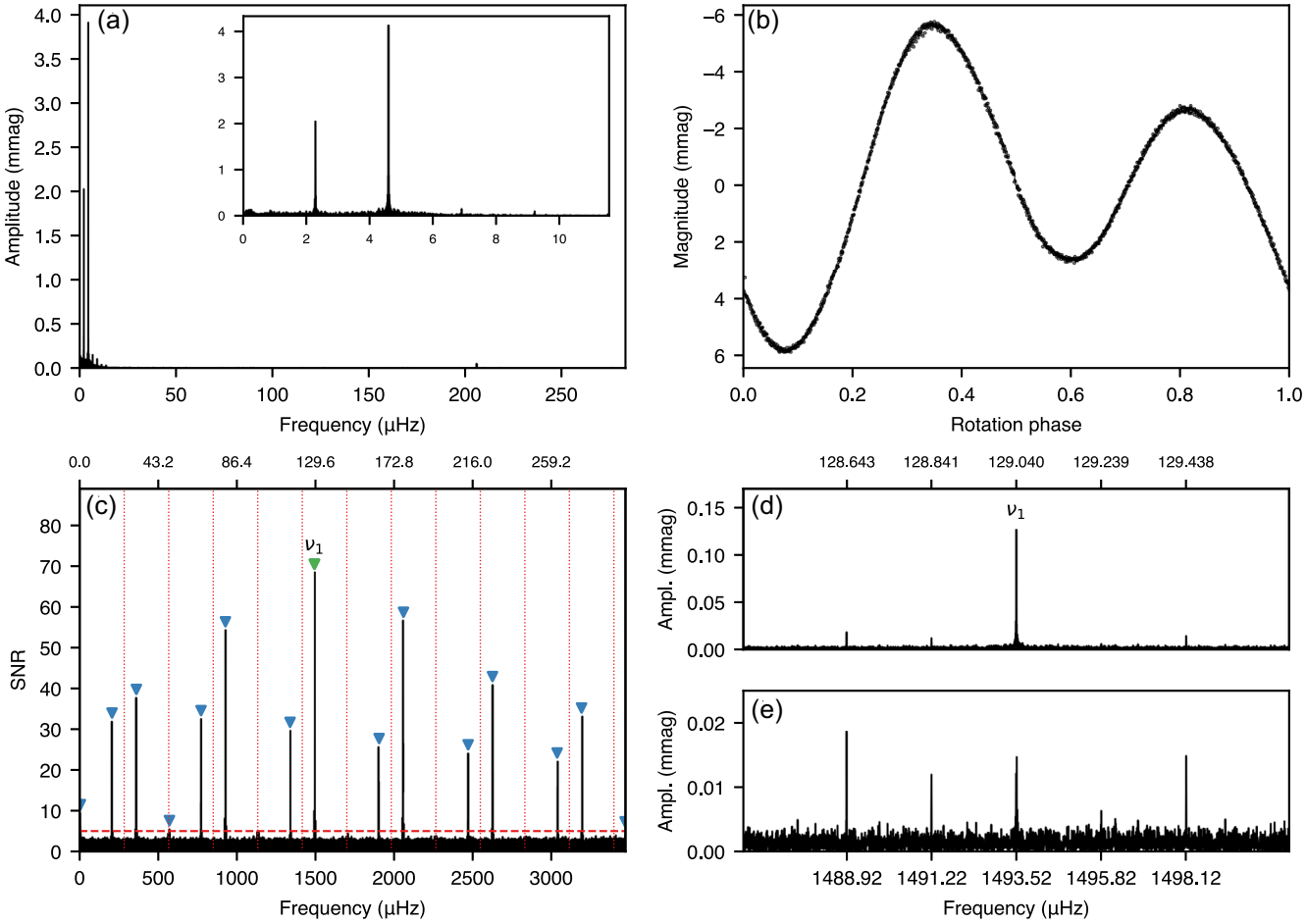

Figure 2. (a) Amplitude spectrum of KIC 6631188 out to the Nyquist frequency of 283.2 μHz. The inset shows the low-frequency region with peaks due to rotation. (b) Light curve folded at the rotation period of 5.03 d and binned at a factor of 50:1. (c) Amplitude spectrum of KIC 6631188 after a high-pass filter has removed the low-frequency signals – the true oscillation frequency of 1493.52 μHz has the highest amplitude (green). All other peaks flagged as aliases above the 5 SNR are marked in blue. The red dashed lines denote integer multiples of the Nyquist frequency. (d) Zoomed region of the primary frequency before, and (e), after pre-whitening ν_1. The residual power in ν_1 is due to frequency variability. The four sidelobes are due to rotational modulation of the pulsation amplitude (see text). The top x-axis, where shown, is the corresponding frequency in d^{-1}.

frequency variability is minimal. This provided a good balance between frequency resolution and variability in the data.

To estimate the large-frequency separation, $\Delta\nu$, defined as the difference in frequency of modes of the same degree and consecutive radial order, we apply the general asteroseismic scaling relation

$$\frac{\Delta\nu}{\Delta\nu_\odot} = \sqrt{\frac{\rho}{\rho_\odot}} = \frac{(M/\mathrm{M}_\odot)^{0.5}(T_\mathrm{eff}/\mathrm{T}_{\mathrm{eff},\odot})^3}{(L/\mathrm{L}_\odot)^{0.75}} \quad (3)$$

with adopted solar values $\Delta\nu_\odot = 134.88 \pm 0.04$ μHz, and $T_{\mathrm{eff},\odot} = 5777$ K (Huber et al. 2011). Using the stellar properties in Table 1, we estimate the large separation as 55.19 ± 7.27 μHz. The separation from the primary frequency ν_1 to ν_2 and ν_3 are 24.86 and 25.18 μHz, respectively, indicating that the observed modes are likely of alternating even and odd degrees. While we cannot determine the degrees of the modes from the LC data alone, it suggests that the primary frequency ν_1 is actually a quintuplet with unobserved positive sidelobes.

If ν_1 is instead a triplet, it would have highly asymmetric rotational sidelobe peak amplitudes which the other modes do not exhibit. Asymmetric sidelobe amplitudes are a signature of the Coriolis effect (Bigot & Dziembowski 2003), but whether this is the sole explanation for such unequal distribution of power in the amplitude spectra cannot be known without follow-up observations. ν_1 is thus more likely to be a quintuplet as the large separation would then be 50.04 μHz, a value much closer to the expected result. The positive suspected sidelobes at frequencies of 1945.46 and 1945.62 μHz have an SNR of 1.16 and 1.78, respectively, well below the minimum level required for confirmation. To this end, we provide a fit to the full quintuplet in Table 2, but note that the frequencies should be treated with caution.

Assuming that ν_2 and ν_3 are triplets, while ν_1 is a quintuplet, we forced the rotational sidelobes to be equally separated from the pulsation mode frequency by the rotation frequency. Lacking the rotational signal from the low-frequency amplitude spectrum, we instead obtained the rotational frequency by examining the variability in amplitudes of the modes themselves. As the star rotates, the observed amplitudes of the oscillations will modulate in phase with the rotation. We provide a full discussion of this phenomenon in Section 5.4. We obtained a rotation frequency of 0.160 ± 0.005 μHz, corresponding to a period of 72.7 ± 2.5 d. We used this amplitude modulation frequency to fit the multiplets by linear least squares to test the oblique pulsator model. By choosing

Table 2. Non-linear least-squares fit of the rotation frequency and the pulsation multiplets. The zero-points of the fits were chosen to be the centre of each light curve. Rotational frequencies, $\nu_{\rm rot}$, are calculated from the low-frequency portion of the unfiltered light curve when available, whereas the oscillation frequencies are calculated on the high-pass filtered light curve. $\delta\nu$ is the difference in frequency between the current and previous row.

KIC	Label	Frequency (μHz)	Amplitude $_{\rm measured}$ (mmag)	Amplitude $_{\rm intrinsic}$ (mmag)	Phase (rad)	$\delta\nu$ (μHz)	$\delta\nu/\nu_{\rm rot}$
6631188	$\nu_{\rm rot}$	2.300 47 ± 0.000 04	2.053 ± 0.016	2.053 ± 0.016			
	$\nu_1 - 2\nu_{\rm rot}$	1488.918 89 ± 0.000 25	0.018 ± 0.001	0.163 ± 0.009	2.171 ± 0.058		
	$\nu_1 - \nu_{\rm rot}$	1491.219 21 ± 0.000 42	0.011 ± 0.001	0.100 ± 0.009	− 2.601 ± 0.095	2.300	1.000
	ν_1	1493.519 47 ± 0.000 04	0.123 ± 0.001	1.119 ± 0.009	0.672 ± 0.009	2.300	1.000
	$\nu_1 + \nu_{\rm rot}$	1495.819 89 ± 0.000 74	0.006 ± 0.001	0.058 ± 0.009	0.906 ± 0.169	2.300	1.000
	$\nu_1 + 2\nu_{\rm rot}$	1498.121 02 ± 0.000 33	0.014 ± 0.001	0.130 ± 0.009	− 2.092 ± 0.074	2.301	1.000
7018170	$\nu_{\rm rot}$	0.1591 ± 0.0054[a]					
	$\nu_1 - 2\nu_{\rm rot}$	1944.982 10 ± 0.001 23	0.008 ± 0.001	0.092 ± 0.013	3.128 ± 0.322		
	$\nu_1 - \nu_{\rm rot}$	1945.142 81 ± 0.000 67	0.015 ± 0.001	0.170 ± 0.013	− 3.038 ± 0.176	0.161	1.010
	ν_1	1945.301 73 ± 0.000 22	0.047 ± 0.001	0.513 ± 0.013	− 2.687 ± 0.058	0.159	0.999
	$\nu_1 + \nu_{\rm rot}$	1945.454 78 ± 0.003 06	0.003 ± 0.001	0.037 ± 0.013	− 4.674 ± 0.806	0.153	0.962
	$\nu_1 + 2\nu_{\rm rot}$	1945.621 68 ± 0.003 33	0.003 ± 0.001	0.034 ± 0.013	− 1.768 ± 0.874	0.167	1.049
	$\nu_2 - \nu_{\rm rot}$	1920.120 72 ± 0.001 41	0.007 ± 0.001	0.082 ± 0.013	0.738 ± 0.369		
	ν_2	1920.278 31 ± 0.000 95	0.011 ± 0.001	0.123 ± 0.013	0.504 ± 0.249	0.158	0.991
	$\nu_2 + \nu_{\rm rot}$	1920.439 44 ± 0.002 47	0.004 ± 0.001	0.047 ± 0.013	0.268 ± 0.648	0.161	1.013
	$\nu_3 - \nu_{\rm rot}$	1970.165 86 ± 0.001 69	0.006 ± 0.001	0.066 ± 0.013	− 1.657 ± 0.444		
	ν_3	1970.324 09 ± 0.001 47	0.007 ± 0.001	0.077 ± 0.013	− 2.795 ± 0.385	0.158	0.995
	$\nu_3 + \nu_{\rm rot}$	1970.483 30 ± 0.001 83	0.006 ± 0.001	0.061 ± 0.013	− 2.552 ± 0.481	0.159	1.001
10685175	$\nu_{\rm rot}$	3.731 18 ± 0.000 01	4.951 ± 0.010	4.951 ± 0.010			
	$\nu_1 - 2\nu_{\rm rot}$	2775.545 47 ± 0.003 38	0.004 ± 0.003	0.191 ± 0.150	1.077 ± 0.800		
	$\nu_1 - \nu_{\rm rot}$	2779.225 90 ± 0.002 03	0.006 ± 0.003	0.337 ± 0.161	− 1.803 ± 0.481	3.680	0.986
	ν_1	2783.008 00 ± 0.000 96	0.013 ± 0.003	0.765 ± 0.173	2.953 ± 0.228	3.782	1.014
	$\nu_1 + \nu_{\rm rot}$	2786.689 62 ± 0.003 00	0.004 ± 0.003	0.266 ± 0.187	0.437 ± 0.708	3.682	0.987
	$\nu_1 + 2\nu_{\rm rot}$	2790.983 95 ± 0.002 84	0.005 ± 0.003	0.310 ± 0.206	− 2.863 ± 0.671	4.294	1.151
11031749	ν_1	1372.717 24 ± 0.000 16	0.0261 ± 0.0006	0.205 ± 0.005	0.899 ± 0.021		
11296437	$\nu_{\rm rot}$	1.624 58 ± 0.000 01	1.705 ± 0.002	1.705 ± 0.002			
	$\nu_1 - \nu_{\rm rot}$	1408.152 04 ± 0.000 44	0.0026 ± 0.0003	0.020 ± 0.002	− 2.229 ± 0.100		
	ν_1	1409.776 71 ± 0.000 02	0.0450 ± 0.0003	0.352 ± 0.002	2.437 ± 0.006	1.625	1.000
	$\nu_1 + \nu_{\rm rot}$	1411.402 13 ± 0.000 49	0.0023 ± 0.0003	0.018 ± 0.002	0.823 ± 0.112	1.625	1.001
	ν_2	126.791 38 ± 0.000 05	0.0222 ± 0.0003	0.0242 ± 0.0003	− 1.716 ± 0.012		
	ν_3	129.151 22 ± 0.000 04	0.0317 ± 0.0003	0.0345 ± 0.0003	2.080 ± 0.008		
11409673	$\nu_{\rm rot}$	0.940 16 ± 0.000 02	0.865 ± 0.006	0.865 ± 0.006			
	$\nu_1 - \nu_{\rm rot}$	2499.985 30 ± 0.001 01	0.021 ± 0.001	0.307 ± 0.018	− 1.571 ± 0.057		
	ν_1	2500.926 65 ± 0.003 21	0.007 ± 0.001	0.097 ± 0.018	0.667 ± 0.199	0.941	1.001
	$\nu_1 + \nu_{\rm rot}$	2501.866 33 ± 0.001 11	0.019 ± 0.001	0.280 ± 0.018	− 1.757 ± 0.069	0.940	0.999

[a]Rotation has been calculated from amplitude modulation of its frequencies (cf. Section 5.4).

Table 3. Linear least-squares fit to the pulsation and force-fitted sidelobes in KIC 6631188. The zero-point for the fit is BJD 2455692.84871, and has been chosen as such to force the first pair of sidelobe phases to be equal.

ID	Frequency (μHz)	Amplitude $_{\rm intrinsic}$ (mmag)	Phase (rad)
$\nu_1 - 2\nu_{\rm rot}$	1488.9185	0.163 ± 0.009	1.579 ± 0.058
$\nu_1 - \nu_{\rm rot}$	1491.2190	0.100 ± 0.009	1.337 ± 0.095
ν_1	1493.5195	1.121 ± 0.009	2.845 ± 0.009
$\nu_1 + \nu_{\rm rot}$	1495.8199	0.058 ± 0.009	1.337 ± 0.167
$\nu_1 + 2\nu_{\rm rot}$	1498.1204	0.130 ± 0.009	2.859 ± 0.075

the zero-point in time such that the phases of the $\pm\nu_{\rm rot}$ sidelobes of ν_1 are equal, we found that ν_1, does not appear to be distorted, and ν_3 only slightly. ν_2 is heavily distorted, as shown by the unequal phases of the multiplet in Table 4.

We can again constrain the inclination and magnetic obliquity angles for the modes. In the case of a pure dipole triplet,

$$\tan i \tan \beta = \frac{A^{(1)}_{+1} + A^{(1)}_{-1}}{A^{(1)}_{0}}, \quad (4)$$

where again $A^{(1)}_{\pm1}$ are the dipole sidelobe amplitudes, and $A^{(1)}_0$ is the amplitude of the central peak. Using Table 4, we find that $\tan i \tan \beta = 1.0 \pm 0.2$, and $\tan i \tan \beta = 1.7 \pm 0.4$ for ν_2, and ν_3, respectively. Using equation (2), we find $\tan i \tan \beta = 2.4 \pm 0.4$ for ν_1, which agrees with ν_3 within the large errors, while disagreeing with ν_2, which appears to be π rad out of phase. We provide a summary of values satisfying these relations in Fig. 3.

4.3 KIC 10685175

KIC 10685175 was detected by manual inspection of the mCP stars from Hümmerich et al. (2018), and was not flagged by the pipeline. The star shows obvious rotational modulation in the low-frequency region of the amplitude spectrum (Fig. 5). The period of rotation, 3.10198 ± 0.00001 d was determined from the low-frequency signal at 0.322 μHz.

To study the roAp pulsations, we subtracted the rotational frequency and its first 30 harmonics. Although the amplitude spectrum is too noisy to reveal *Kepler* orbital sidelobe splitting, the true peak is evident as the signal with the highest power: 2783.01 μHz. This frequency lies close to a multiple of the *Kepler*

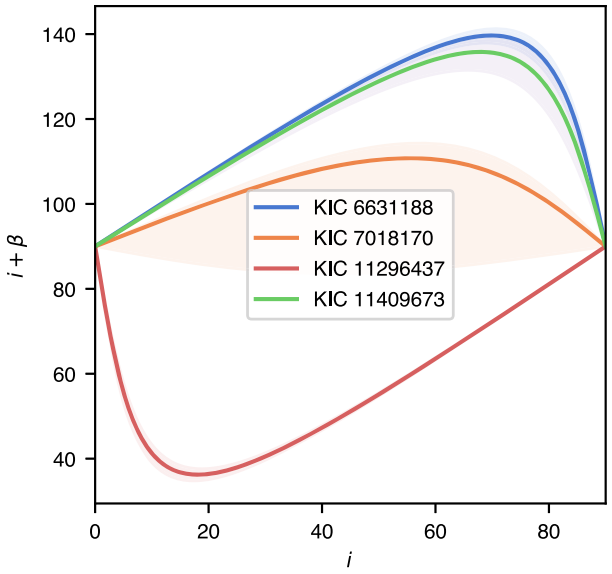

Figure 3. Possible $i + \beta$ combinations for the roAp stars where analysis of the multiplets allows us to set constraints on their geometry. The shaded region marks the uncertainty. In stars for which $i + \beta > 90^\circ$, both magnetic poles are observed. For KIC 7018170, only the primary ν_1 solution has been shown. KIC 10685175 has been omitted as its uncertainty dominates the figure.

sampling rate, and thus has a highly diminished amplitude. The primary frequency appears to be a quintuplet split by the rotational frequency. However, the low SNR of the outermost rotational sidelobes necessitates careful consideration. The outer sidelobes, at frequencies of 2775.55 and 2790.47 μHz have an SNR of 1.28 and 0.49, respectively. Similar to KIC 7018170, we provide a fit to the full suspected quintuplet in Table 2, but again note that the frequencies of the outermost sidelobes should be treated with caution. If we are to assume that the pulsation is a triplet, while ignoring the outer sidelobes, then equation (4) yields a value of $\tan i \tan \beta = 0.9 \pm 0.4$, implying that $i + \beta < 90^\circ$ and that only one pulsation pole is observed. The large uncertainty however indicates that either one or two poles can be observed if the pulsation is modelled as a triplet. On the other hand, if we consider the star as a quadrupole pulsator, we obtain a value of $\tan i \tan \beta = 1.7 \pm 1.6$, a result almost completely dominated by its uncertainty.

We again investigate the distortion of the mode by assuming that the multiplet is split by the rotation frequency, and find that all phases agree within error, implying minimal distortion of the mode (Table 5). However, it should be noted that the low SNR of the spectrum greatly inflates the uncertainties on the amplitudes and phases of the fit.

4.4 KIC 11031749

KIC 11037149 does not appear to demonstrate spot-based amplitude modulation in its light curve (Fig. 6), or does it show signs of rotational frequency splitting – consistent with a lack of rotational modulation. Despite this, it is clear that it possesses unusual chemical abundances of Sr, Cr, and Eu from its spectrum (Section 5.2). We theorize two possibilities behind the lack of observable modulation. If the angles of inclination or magnetic obliquity are close to 0°, no modulation would be observed since the axis of rotation is pointing towards *Kepler*. However, this assumes that the chemical abundance spots are aligned over the magnetic poles, which has been shown to not always be the case (Kochukhov et al. 2004). Another possibility is that the period of rotation could be much longer than the time-base of the *Kepler* LC data. While the typical rotational period for A-type stars is rather short (Royer, Zorec & Gómez 2007; Royer 2009; Murphy 2015b), the rotation for Ap types can exceed even 10 yr due to the effects of magnetic braking (Landstreet & Mathys 2000). Indeed, a non-negligible fraction of Ap stars are known to have rotational periods exceeding several centuries (Mathys 2015), and so it is possible for the star to simply be an extremely slow rotator.

The aliased signal of the true pulsation is visible even in the unfiltered LC data (Fig. 6). After filtering, we identified one pulsation frequency (ν_1: 1372.72 μHz), and provide a fit in Table 2. With no clear multiplet structure around the primary frequency, we are unable to constrain the inclination and magnetic obliquity within the framework of the oblique pulsator model. Indeed, without any apparent low-frequency modulation we are unable to even provide a rotation period. This represents an interesting, although not unheard of challenge for determining the rotation period. Since the photometric and spectral variability originate with the observed spot-based modulation, neither method can determine the rotation period without a longer time-base of observations. Regardless, we include KIC 11031749 in our list of new roAp stars as it satisfies the main criterion of exhibiting both rapid oscillations and chemical abundance peculiarities.

4.5 KIC 11296437

KIC 11296437 is a known rotationally variable star (Reinhold et al. 2013), whose period of rotation at 7.12433 ± 0.00002 d is evident in the low-frequency region of the amplitude spectrum (Fig. 7). Folding the light curve on this period shows only a single spot or set of spots, implying that $i + \beta < 90^\circ$.

The primary pulsation frequency was found to be 1409.78 μHz in the high-pass filtered light curve. This mode shows two sidelobes split by 1.625 μHz which is in good agreement with the rotation frequency. Two low-frequency modes, ν_2 and ν_3, are also present below the Nyquist frequency, at 126.79 and 129.15 μHz, respectively. These modes are clearly non-aliased pulsations, as they are not split by the *Kepler* orbital period. However, neither of them are split by the rotational frequency. We provide a fit to these frequencies in Table 2.

We apply the oblique pulsator model to ν_1 by assuming the mode is split by the rotation frequency, and find that all three phases agree within error, implying that ν_1 is not distorted. The same test cannot be applied to ν_2 and ν_3 due to their lack of rotational splitting. We can further constrain the geometry of the star by again considering the sidelobe amplitude ratios (equation 4). Using the values in Table 6, we find that $\tan i \tan \beta = 0.11 \pm 0.01$, and provide a summary of angles satisfying these values in Fig. 3, which demonstrates that only one pulsation pole should be observed over the rotation cycle ($i + \beta < 90^\circ$).

KIC 11296437 is highly unusual in that it displays both high-frequency roAp pulsations and low-frequency *p*-mode pulsations that are typically associated with δ Scuti stars. A lack of rotational splitting in the low-frequency modes suggests that the star might be a binary composed of a δ Scuti and roAp star component. If KIC 11296437 is truly a single-component system, then it would pose a major challenge to current theoretical models of roAp stars. In particular, the low-frequency modes at 126.79 and 129.15 μHz are expected to be damped by the magnetic field according to previous

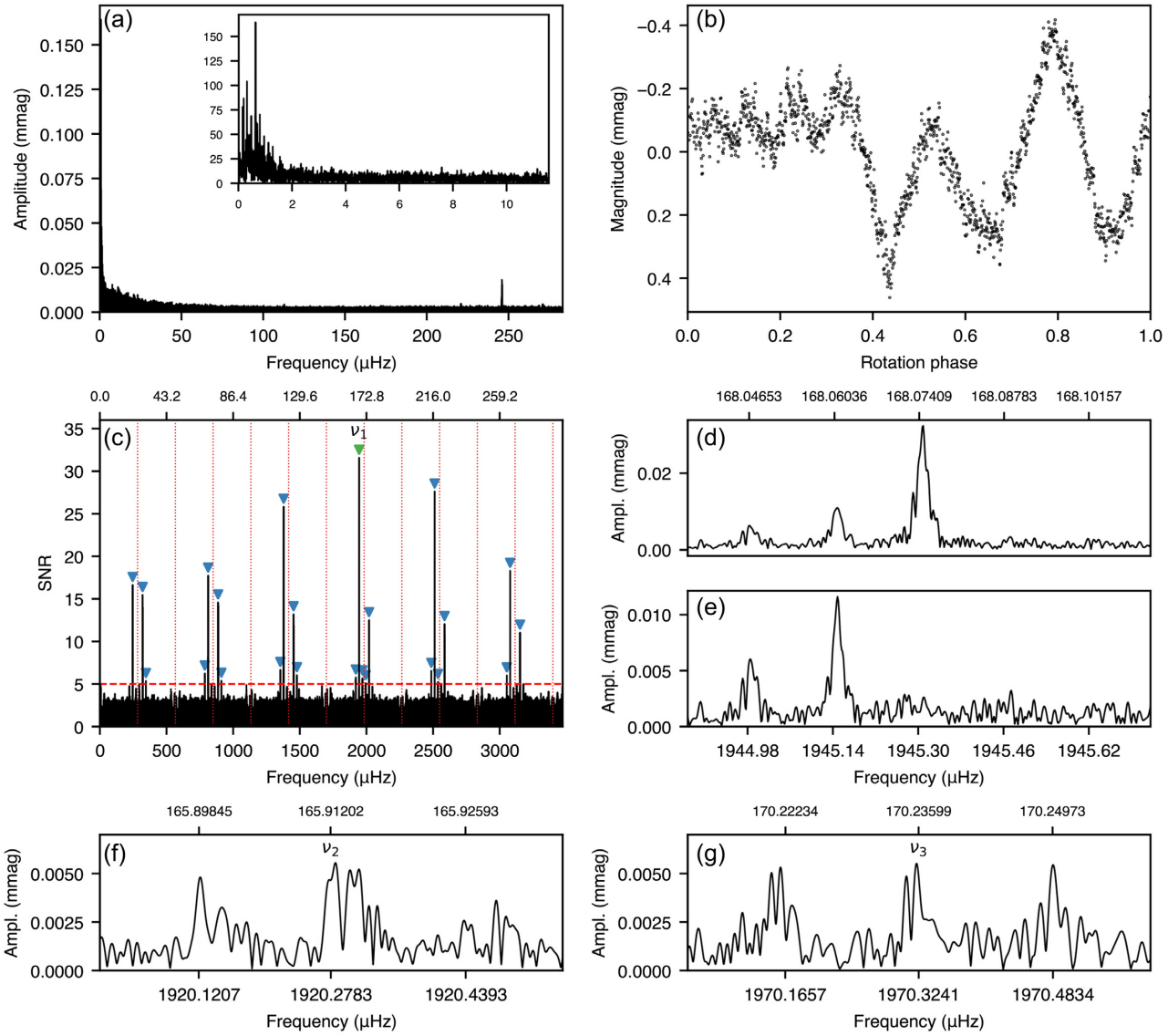

Figure 4. Same as in Fig. 2 for KIC 7018170. In (a) however, the long-period rotational modulation has been largely removed by the PDCSAP flux pipeline leading to a jagged light curve (b). Panels (f) and (g) show the secondary frequencies ν_2 and ν_3 extracted after manual inspection of the filtered light curve.

Table 4. Linear least-squares fit to the pulsation and force-fitted sidelobes in KIC 7018170. The zero-point for the fit is BJD 2455755.69582, and has been chosen as such to force the sidelobe phases of ν_1 to be equal.

ID	Frequency (μHz)	Amplitude $_{\text{intrinsic}}$ (mmag)	Phase (rad)
$\nu_1 - 2\nu_{\text{rot}}$	1944.98350	0.090 ± 0.013	−2.799 ± 0.141
$\nu_1 - \nu_{\text{rot}}$	1945.14259	0.172 ± 0.013	−3.080 ± 0.074
ν_1	1945.30169	0.510 ± 0.013	−2.683 ± 0.025
$\nu_1 + \nu_{\text{rot}}$	1945.46079	0.031 ± 0.013	−3.080 ± 0.403
$\nu_1 + 2\nu_{\text{rot}}$	1945.61988	0.033 ± 0.013	−2.170 ± 0.389
$\nu_2 - \nu_{\text{rot}}$	1920.11921	0.081 ± 0.013	0.407 ± 0.161
ν_2	1920.27831	0.122 ± 0.013	0.522 ± 0.107
$\nu_2 + \nu_{\text{rot}}$	1920.43741	0.046 ± 0.013	−0.109 ± 0.283
$\nu_3 - \nu_{\text{rot}}$	1970.16500	0.066 ± 0.013	−1.828 ± 0.192
ν_3	1970.32410	0.076 ± 0.013	−2.786 ± 0.165
$\nu_3 + \nu_{\text{rot}}$	1970.48320	0.061 ± 0.013	−2.562 ± 0.206

theoretical modelling (Saio 2005). KIC 11296437 would be the first exception to this theory amongst the roAp stars.

On the other hand, it would also be highly unusual if KIC 11296437 were a binary system. It is rare for Ap stars to be observed in binaries, and much more so for roAp stars. Currently, there is one known roAp star belonging to a spectroscopic binary (Hartmann & Hatzes 2015), with several other suspected binaries (Schöller et al. 2012). Stellar multiplicity in roAp stars is important for understanding their evolutionary formation and whether tidal interactions may inhibit their pulsations.

4.6 KIC 11409673

KIC 11409673 is a peculiar case, as it has previously been identified as an eclipsing binary, and later a heartbeat binary (Kirk et al. 2016). We note that a radial velocity survey of heartbeat stars has positively identified KIC 11409673 as a roAp star (Shporer et al.

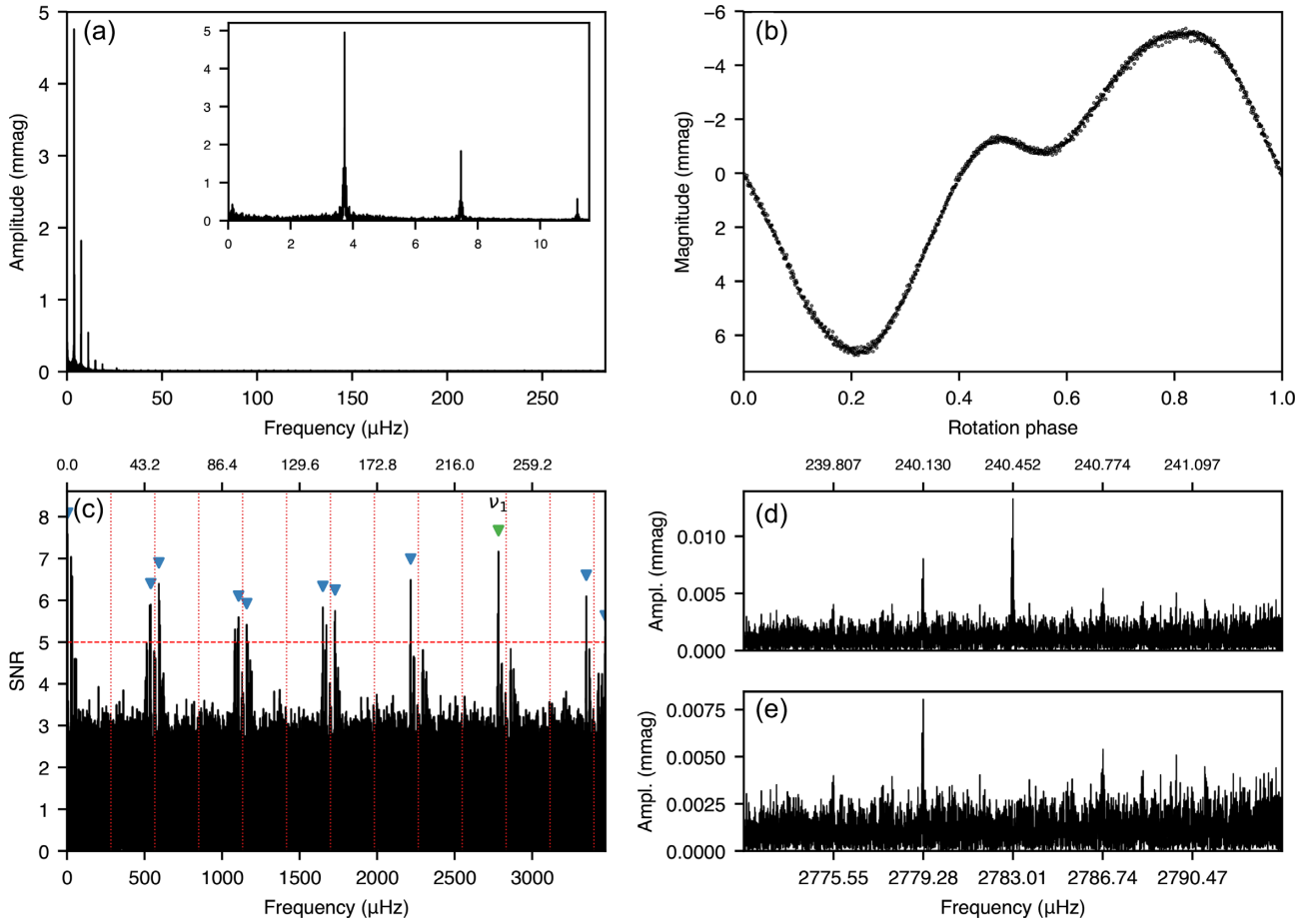

Figure 5. (a) Amplitude spectrum of KIC 10685175 out to the nominal Nyquist frequency. The inset shows the low-frequency region of the spectrum corresponding to the rotation frequency. (b) Light curve folded at the rotation period of 5.03 d and binned at a ratio of 50:1. (c) Amplitude spectrum of KIC 10685175 after pre-whitening – the true oscillation frequency of 2783.00 μHz can be observed as the signal of maximum amplitude (green). All other peaks flagged as aliases above the 5 SNR are marked in blue. The red dashed lines denote integer multiples of the Nyquist frequency. (d) Zoomed region of the primary frequency before, and (e), after pre-whitening ν_1.

Table 5. Linear least-squares fit to the pulsation and force-fitted sidelobes in KIC 10685175. The zero-point for the fit is BJD 2455689.78282, and has been chosen as such to force the first pair of sidelobe phases to be equal.

ID	Frequency (μHz)	Amplitude $_{\text{intrinsic}}$ (mmag)	Phase (rad)
$\nu_1 - 2\nu_{\text{rot}}$	2775.545 64	0.192 ± 0.150	0.842 ± 0.782
$\nu_1 - \nu_{\text{rot}}$	2779.276 82	0.432 ± 0.161	0.324 ± 0.373
ν_1	2783.008 00	0.764 ± 0.173	0.585 ± 0.226
$\nu_1 + \nu_{\text{rot}}$	2786.739 19	0.243 ± 0.187	0.324 ± 0.772
$\nu_1 + 2\nu_{\text{rot}}$	2790.470 37	0.099 ± 0.204	0.049 ± 2.051

2016). Here we provide independent confirmation of this result through super-Nyquist asteroseismology, as their result has been ignored in later catalogues of roAp stars. KIC 11409673 has a clear low-frequency variation at 0.94 μHz, corresponding to a rotational period of 12.3107 ± 0.0003 d. Similar to KIC 6631188, the low-frequency region is dominated by a higher amplitude signal at $2\nu_{\text{rot}}$ consistent with observations of the double-wave nature, as seen in Fig. 8. The rotation period of 12.31 d is found by folding the light curve, and is confirmed after high-pass filtering the light curve and examining the triplet centred around the primary frequency of 2500.93 μHz. Similar to KIC 7018170, KIC 11409673 exhibits strong frequency variation which negatively affects the shape of the multiplets. We thus split the LC data into four equally spaced sections and analysed the multiplet separately in each section. This reduced the issues arising from frequency variation, despite leading to a decrease in frequency resolution. The results of the least-squares analysis for the first section of data are presented in Table 2.

Again, applying the oblique pulsator model by assuming that the sidelobes be separated from the primary frequency by the assumed rotation frequency, we fit each section of data via least squares. By choosing the zero-point in time such that the phases of the sidelobes are equal, we are able to show that the mode is not distorted, as the three phases agree within error. This is the case for all four separate fits. The results of this test for the first section of the data are shown in Table 7, with the remaining sections in Table A1. We find that $\tan i \tan \beta = 6.1 \pm 1.1$ using equation (4) for the first section of data, implying that both spots are observed in agreement with the light curve.

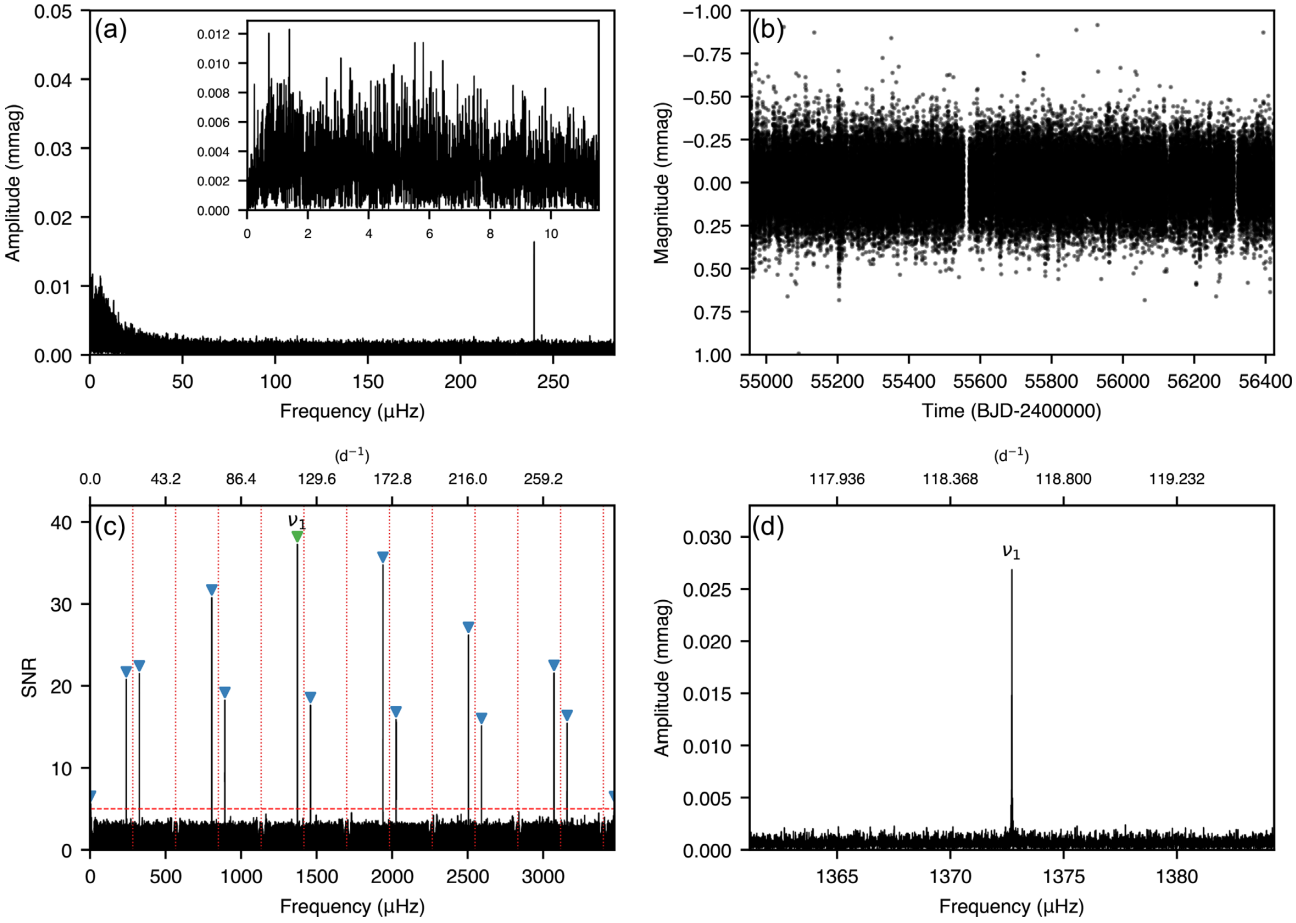

Figure 6. Same as Fig. 2 for KIC 11031749. No rotation signal can be observed in either (a) the low-frequency amplitude spectrum or (d) rotational splitting. We provide the full 4 yr light curve in lieu of a folded light curve (b).

5 DISCUSSION

5.1 Acoustic cut-off frequencies

As discussed in Section 1, several roAp stars are known to oscillate above their theoretical acoustic cut-off frequency ($\nu_{\rm ac}$). The origin of the pulsation mechanism in these superacoustic stars remains unknown, and presents a significant challenge to theoretical modelling. We therefore calculate whether the stars presented here oscillate above their theoretical acoustic cut-off frequency following the relation

$$\frac{\nu_{\rm ac}}{\nu_{\rm ac,\odot}} = \frac{M/{\rm M}_\odot (T_{\rm eff}/{\rm T}_{\rm eff,\odot})^{3.5}}{L/{\rm L}_\odot}, \quad (5)$$

where $\nu_{\rm ac,\odot} = 5300\,\mu$Hz is the theoretical acoustic cut-off frequency of the Sun (Jiménez, García & Pallé 2011). Using the values provided in Table 1, we find that KIC 7018170 and KIC 11409673 both oscillate above their theoretical limit (1739.5 and 2053.7 μHz, respectively). The remaining stars do not oscillate above their theoretical acoustic cut-off frequency. KIC 11031739, however, lies almost exactly on the border of the acoustic cut-off frequency within the errors.

5.2 Spectral classification

The LAMOST (Large Sky Area Multi-Object Fiber Spectroscopic Telescope; Zhao et al. 2012) survey has collected low-resolution spectra between 3800 and 9000 Å for objects in the *Kepler* field. We obtained LAMOST spectra from the 4th Data Release (DR4). All stars presented here have at minimum one low-resolution spectrum available from LAMOST. However, the spectrum of KIC 6631188 is of unusable SNR. We thus obtained a high-resolution spectrum of KIC 6631188 on 2019 April 17 using the HIRES spectrograph (Vogt et al. 1994) at the Keck-I 10-m telescope on Maunakea observatory, Hawai'i. The spectrum was obtained and reduced as part of the California Planet Search queue (CPS; Howard et al. 2010). We obtained a 10-min integration using the C5 decker, resulting in an S/N per pixel of 30 at ∼6000 Å with a spectral resolving power of $R \sim 60\,000$. This spectrum has been down-sampled to match the MK standard spectrum.

Fig. 9 presents the spectra of KIC 6631188, KIC 7018170, KIC 11031749, KIC 11296437, and KIC 11409673, with MK standard stars down-sampled to match the resolution of either the HIRES or LAMOST via the SPECTRES package (Carnall 2017). KIC 10685175 has a pre-existing spectral classification of A4 V Eu (Hümmerich et al. 2018), and thus is not re-classified in this work.

In KIC 6631188, there is a strong enhancement of Sr II at 4077 and 4215 Å. The 4111 Å line of Cr II is present, which is used to confirm a Cr peculiarity, but the strongest line of Cr II 4172 Å line is not enhanced. The hydrogen lines look narrow for a main-sequence star, but the metal lines are well bracketed by A9 V and F1 V. We place this star at F0 V Sr.

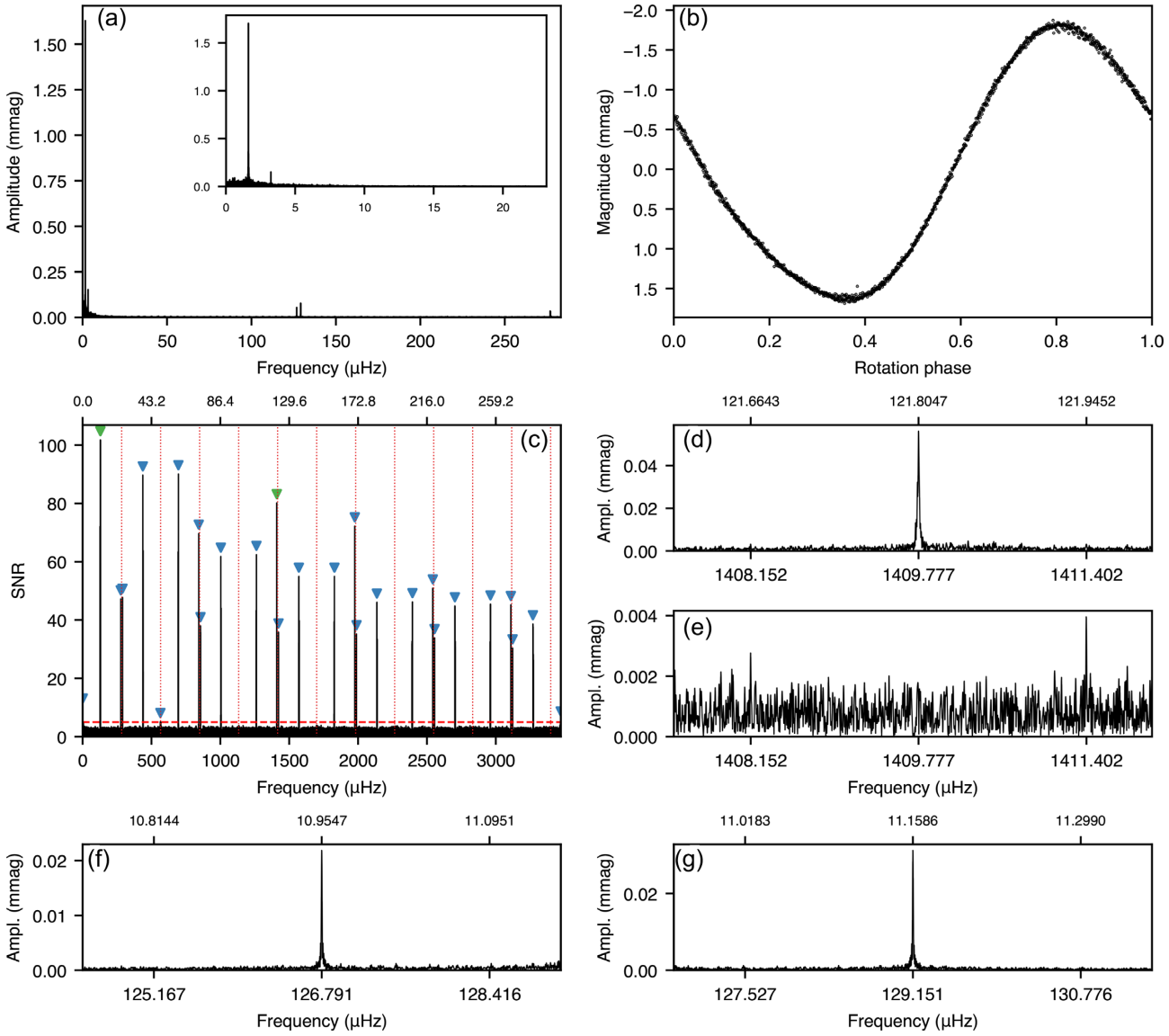

Figure 7. Same as Fig. 2 for KIC 11296437. In the SNR periodogram, it is not always the case that the power distribution in the super-Nyquist regime will ensure that the highest amplitude frequency will also be the highest SNR frequency.

Table 6. Linear least-squares fit to the pulsation and force-fitted sidelobes in KIC 11296437. The zero-point for the fit is BJD 2455690.64114.

ID	Frequency (μHz)	Amplitude $_{\text{intrinsic}}$ (mmag)	Phase (rad)
$\nu_1 - \nu_{\text{rot}}$	1408.152 13	0.020 ± 0.002	−0.678 ± 0.117
ν_1	1409.776 71	0.352 ± 0.002	−0.681 ± 0.007
$\nu_1 + \nu_{\text{rot}}$	1411.401 29	0.018 ± 0.002	−0.678 ± 0.131

KIC 7018170 shows evidence of chemical peculiarities which are only mild, but the spectrum is of low SNR. The 4077 Å line is very strong, which is indicative of an overabundance of Sr or Cr or both, but matching peculiarities in other lines of these elements are less clear. Sr II at 4215 Å is marginally enhanced, and the 4111 and 4172 Å lines of Cr II are also only marginally enhanced. The Eu II line at 4205 Å is significantly enhanced and is matched with a small enhancement at 4128–4132 Å. We place KIC 7018170 as a F2 V (SrCr)Eu type star.

The Ca II K line in KIC 11031749 is broad and a little shallow, typical of magnetic Ap stars. The 4077 Å line is very strong, suggesting enhancement of Sr and/or Cr. A mild enhancement of other Sr and Cr lines suggests both are contributing to the enhancement of the 4077 Å line. There is mild enhancement of the Eu II 4205 Å line and the 4128–4132 Å doublet suggesting Eu is overabundant. It is noteworthy that the Ca I 4226 Å line is a little deep. We thus classify KIC 11031749 as F1 V SrCrEu.

In KIC 11296437, there is a strong enhancement of Eu II at 4130 and 4205 Å. There is no clear enhancement of Sr II at 4216 Å but a slightly deeper line at 4077 Å which is also a line of Cr II. The 4111 Å line of Cr II is present, which is used to confirm a Cr peculiarity, but the 4172 Å line does not look enhanced which is normally the strongest line. The hydrogen lines look narrow for a main-sequence

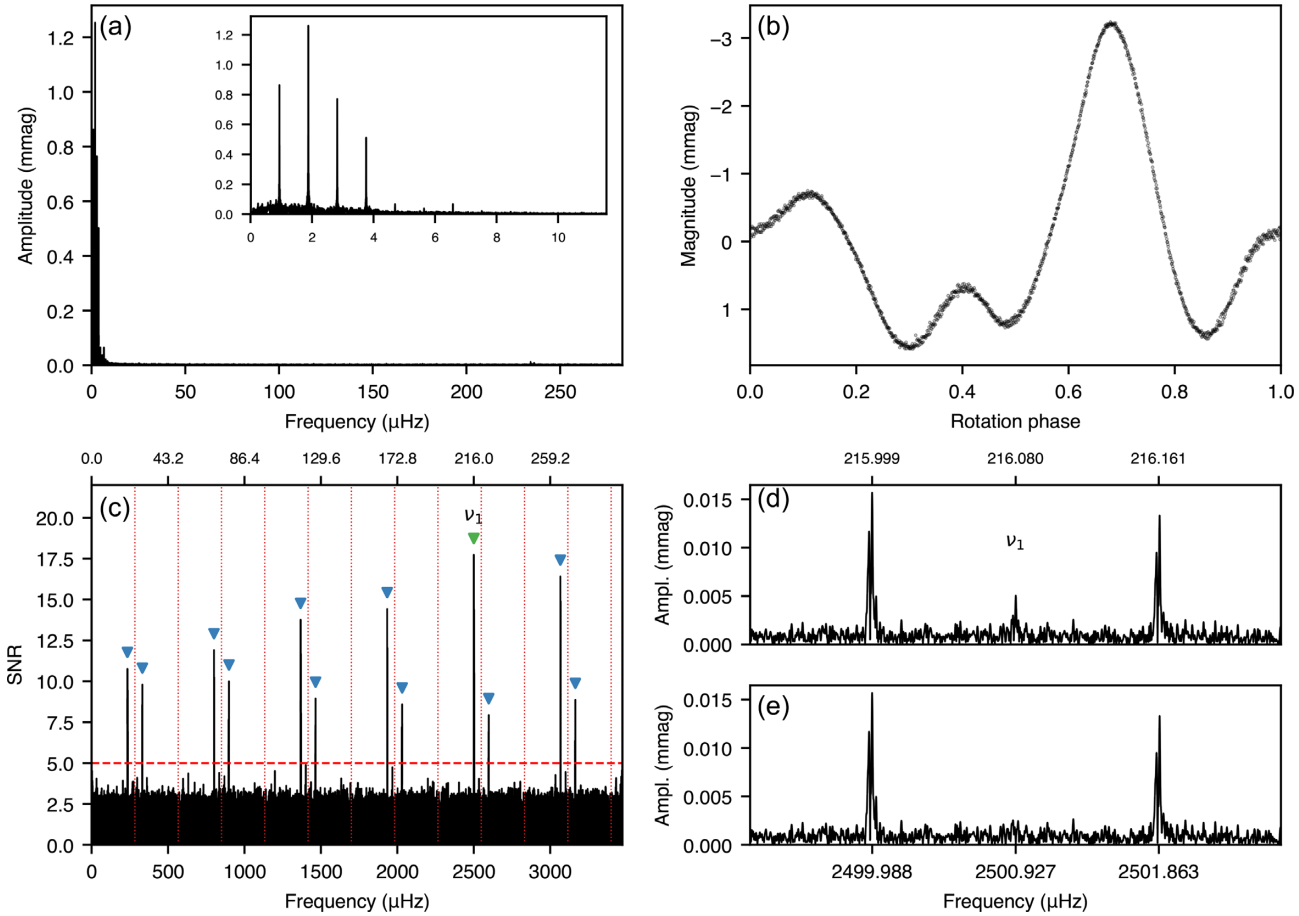

Figure 8. (a) Amplitude spectrum of KIC 11409673 out to the nominal Nyquist frequency. The inset shows the low-frequency region of the spectrum corresponding to the rotation frequency. (b) Light curve folded and binned at a ratio of 50:1. (c) Amplitude spectrum after a high-pass filter has removed the low-frequency signals – the true oscillation frequency can be observed as the signal of maximum amplitude (green). All other peaks flagged as aliases above the 5 SNR are marked in blue. The red dashed lines denote integer multiples of the Nyquist frequency. (d) Zoomed region of the primary frequency before, and (e), after pre-whitening ν_1. The top x-axis, where available, is the corresponding frequency in d^{-1}.

Table 7. Linear least-squares fit to the pulsation and force-fitted sidelobes in KIC 11409673. The zero-point for the fit is BJD 2455144.43981. The data have been split into four equally spaced sets, with the sidelobes force-fitted in each set. We show only the results of the first-set below and provide the rest in Appendix A. The results for each set are similar, and agree within the errors.

ID	Frequency (μHz)	Amplitude $_{\text{intrinsic}}$ (mmag)	Phase (rad)
$\nu_1 - \nu_{\text{rot}}$	2499.986 45	0.306 ± 0.018	1.0173 ± 0.0579
ν_1	2500.926 65	0.097 ± 0.018	1.1551 ± 0.1834
$\nu_1 + \nu_{\text{rot}}$	2501.866 84	0.280 ± 0.018	1.0173 ± 0.0632

star, but the metal lines are well bracketed by A7 V and F0 V. We place this star at A9 V EuCr.

For KIC 11409673, there is enhanced absorption at 4216 Å which is a classic signature of a Sr overabundance in an Ap star. This is usually met with an enhancement in the 4077 Å line, but that line is also a line of Cr. The 4077 Å line is only moderately enhanced, but enough to support a classification of enhanced Sr. Since the 4172 Å line is normal, it appears that Cr is not enhanced. Other Cr lines cannot be relied upon at this SNR. Since the Eu II 4205 Å absorption line is strong, it appears that Eu is overabundant. There is no other evidence for a Si enhancement. The Ca II K line is a little broad and shallow for A9, which suggests mild atmospheric stratification typical of magnetic Ap stars. The hydrogen lines are a good fit intermediate to A7 and F0. We thus classify this star as A9 V SrEu.

5.3 Positions in the H–R diagram

To place our sample on the H–R diagram (Fig. 10), we derived new stellar tracks based on the models of Cunha et al. (2013). We performed linear, non-adiabatic pulsation calculations for a grid of models covering the region of the HR diagram where roAp stars are typically found. We considered models with masses between 1.4 and 2.5 $M_\odot$, in steps of 0.05 $M_\odot$, and fixed the interior chemical composition at $Y = 0.278$ and $X = 0.705$.

The calculations followed closely those described for the polar models discussed in Cunha et al. (2013). The polar models consider that envelope convection is suppressed by the magnetic field, a condition required for the excitation by the opacity mechanism of high radial order modes in roAp stars. Four different cases were considered for each fixed effective temperature and luminosity in

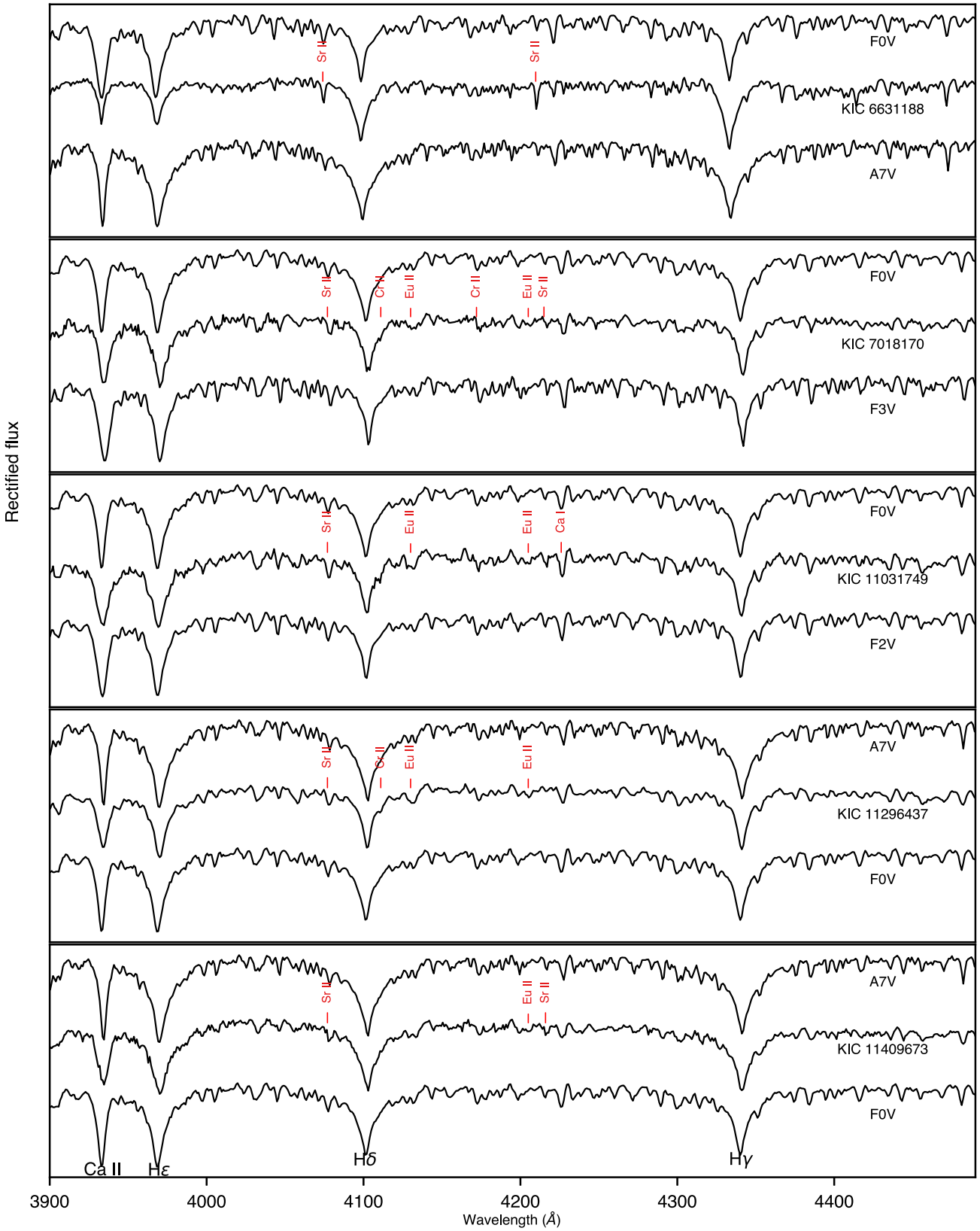

Figure 9. Keck and LAMOST spectra of KIC 6631188, KIC 7018170, KIC 11031749, KIC 11296437, and KIC 11409673 from top to bottom. MK standard spectra have been down-sampled to match the LAMOST resolution. MK standard spectra have been obtained from https://web.archive.org/web/20140717065550/ http://stellar.phys.appstate.edu/Standards/std1_8.html.

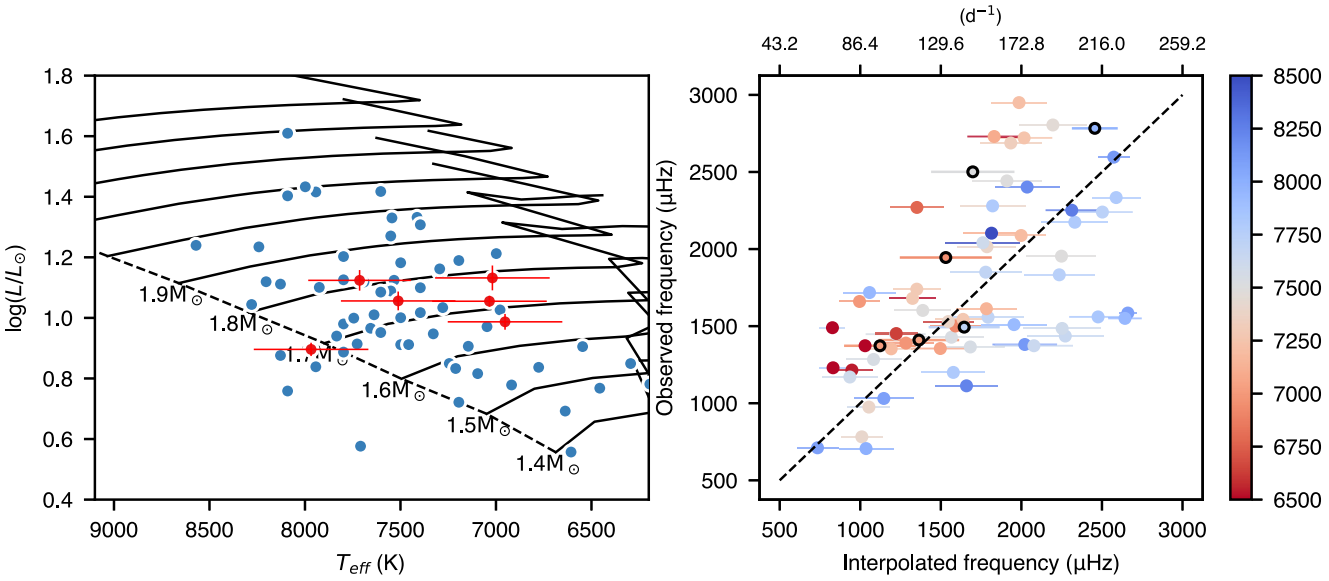

Figure 10. Left-hand panel: Positions of the previously known (blue) and new roAp stars (red) discussed in this paper. Uncertainties have only been shown on the new roAp stars for clarity. Although stellar tracks are computed in 0.05-$M_\odot$ intervals, only every second track has been displayed here. Right-hand panel: Interpolated and observed frequencies from pulsation modelling of the roAp stars, coloured by effective temperature. The observed frequencies are taken as the signal of highest amplitude. Circles mark previously known roAp stars, whereas outlined circles mark the six new stars. Uncertainties on the interpolated frequencies are obtained through a Monte Carlo simulation.

the grid. The first case considered an equilibrium model with a surface helium abundance of $Y_{\rm surf} = 0.01$ and an atmosphere that extends to a minimum optical depth of $\tau_{\rm min} = 3.5 \times 10^{-5}$. For this case the pulsations were computed with a fully reflective boundary condition. The other three cases considered were in all similar to this one, except that the above options were modified one at a time to: $Y_{\rm surf} = 0.1$; $\tau_{\rm min} = 3.5 \times 10^{-4}$; transmissive boundary condition (see Cunha et al. 2013, for further details on the models). We provide a summary of these models in Table 8. We note that the impact of the choice of Y and X on the frequencies of the excited oscillations is negligible compared to the impact of changing the aspects of the physics described above.

For each fixed point in the track we calculated the frequency of maximum growth rate as a comparison to our observed frequencies. The observed frequency was assumed to be the mode of highest linear growth rate. However, it should be noted that this may not necessarily be the case. Using these tracks, we performed linear interpolation to obtain an estimate of the masses and frequencies derived from modelling. Uncertainties on the masses have been artificially inflated to account for uncertainties in metallicity, temperature, and luminosity (0.2, 0.1, and 0.05 $M/M_\odot$ respectively), following Murphy et al. (2019). An extra error component of 0.1 $M/M_\odot$ is included to account for unknown parameters in the stellar modelling, such as overshooting and mixing length. These four contributions are combined in quadrature, yielding a fixed uncertainty of 0.25 $M/M_\odot$. Frequency interpolation is performed for each model (1 through 4), with the plotted value being the median of these results. The uncertainty in the interpolation of both frequency and mass is obtained from a Monte Carlo simulation sampled from the uncertainty in the temperature and luminosity of the stars. We show the results of the positions in the H–R diagram and comparison of interpolated frequencies in Fig. 10.

For frequencies below ~1800 μHz the agreement between theory and observations is reasonable, albeit with discrepancies on a star-by-star case that may be due to an incomplete modelling of the physics of these complex stars. However, for stars with higher characteristic frequencies there seems to be two distinct groups, one lying below and the other clearly above the 1:1 line. Coloured by temperature, we note that the group lying above the 1:1 line tends to be cooler in general. The suppression of envelope convection is key to the driving of roAp pulsations by the opacity mechanism. As it is harder for suppression to take place in the coolest evolved stars, one may question whether an additional source of driving is at play in these stars. In fact, it has been shown in a previous work that the driving of the very high-frequency modes observed in some well-known roAp stars cannot be attributed to the opacity mechanism. It was argued that they may, instead, be driven by the turbulent pressure if envelope convection is not fully suppressed (Cunha et al. 2013). Whether that mechanism could contribute also to the driving of the modes observed in the stars laying clearly above the 1:1 line on the right-hand panel of Fig. 10 is something that should be explored in future non-adiabatic modelling of roAp stars.

5.4 Intrinsic amplitude and phase variability

Many of the known roAp stars have shown significant variation in the amplitudes and phases of their pulsation frequencies over the observation period. To examine this variability in our sample, we conducted a time and frequency domain analysis where a continuous amplitude spectrum was generated by sliding a rectangular window across the light curve. The Fourier amplitude and phase were then calculated within the window at each point. For each star, the window length was chosen to be $100/\nu_1$ d in width to minimize phase and amplitude uncertainty whilst correctly sampling the frequency. Both rectangular and Gaussian windows were tested and found to have minimal difference in the resultant amplitudes. Before calculating the variability, the rotational frequency and

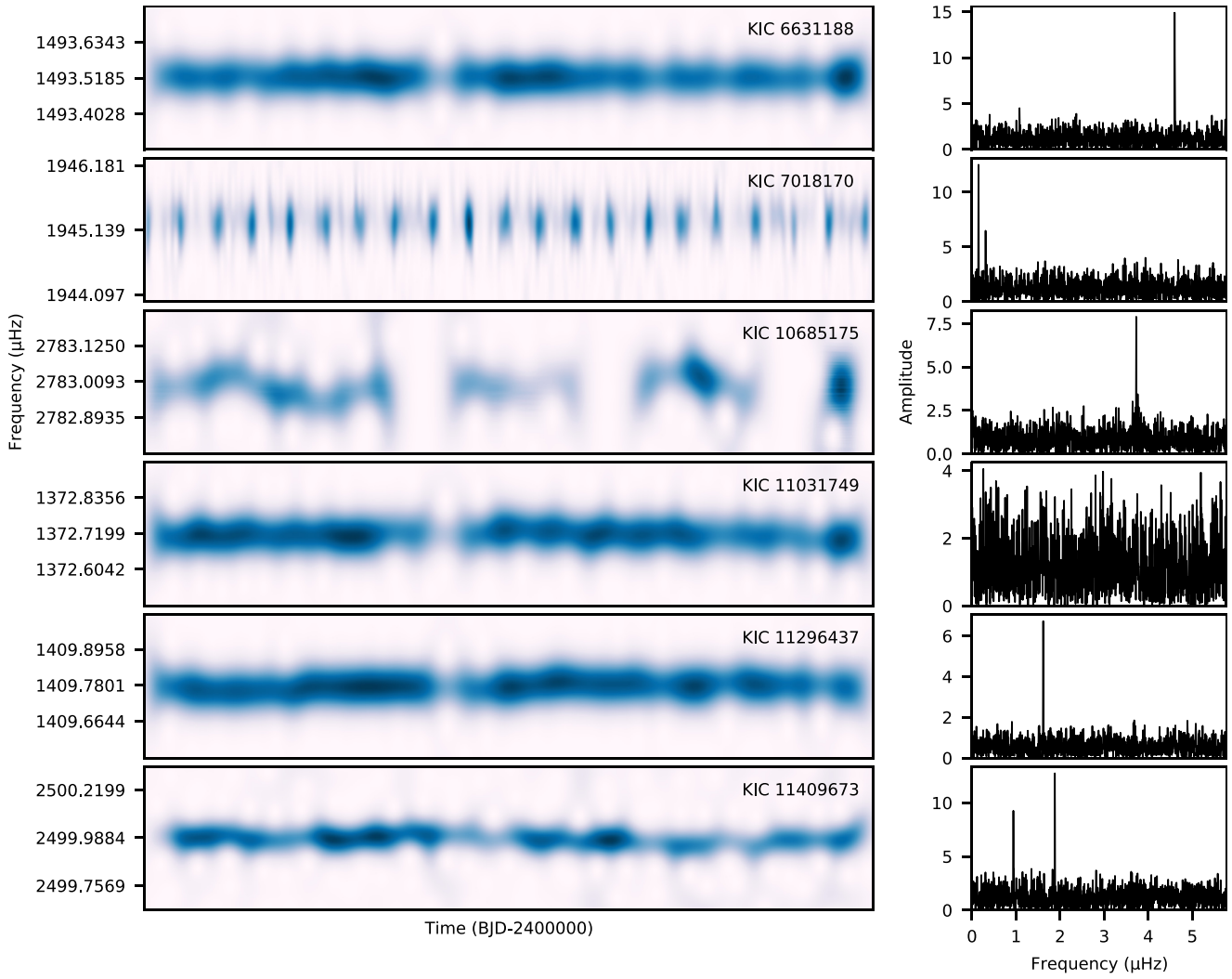

Figure 11. Time and frequency domain analysis of the primary frequencies for each of the roAp stars, where the colour shows the normalized amplitude of the signal. The amplitude spectra (right) are obtained by taking the periodogram of the wavelet at the primary frequency, and are arbitrarily normalized. All but KIC 11031749 show strong frequencies in agreement the spot-based rotational modulation of the light curve, confirming their oblique pulsating nature. The wavelet for KIC 11409673 is taken from the sidelobe frequency $\nu_1 - \nu_{\rm rot}$ due to the central frequency being of low amplitude. The gaps in KIC 10685175 are due to missing quarters in the *Kepler* photometry.

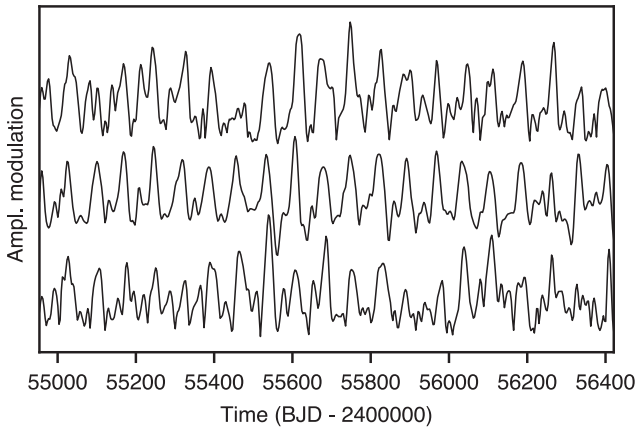

Figure 12. Amplitude modulation of the modes ν_1, ν_2, and ν_3 in KIC 7018170 from top to bottom. All three modes are modulated in phase with each-other, in agreement with the oblique pulsator model.

corresponding harmonics were pre-whitened manually to minimize any potential frequency beating.

Amplitude modulation of the normal modes provides a measure of the rotation period of these stars and confirms the nature of their oblique pulsations. If the pulsation amplitudes goes to zero, then a node crosses the line of sight and is observed, and (for a dipole mode) the pole is at 90° to the line of sight. However, if the geometry is such that the amplitude never goes to zero (e.g. α Cir), then we must always see a pole. This leads to a periodic modulation of the pulsation amplitude, which is different to the spot-based rotational modulation seen in the light curves of Ap stars in general. Similarly, a π rad phase change should be observed in the phase of the frequency whenever a node crosses the line of sight. The continuous amplitude spectrum and corresponding rotational signal are shown in Fig. 11. The rotation signal was obtained by examining the amplitude spectrum of the modulation along the primary frequency of each star.

KIC 6631188 has obvious low-frequency modulation in its light curve, making identification of the rotation period straightforward

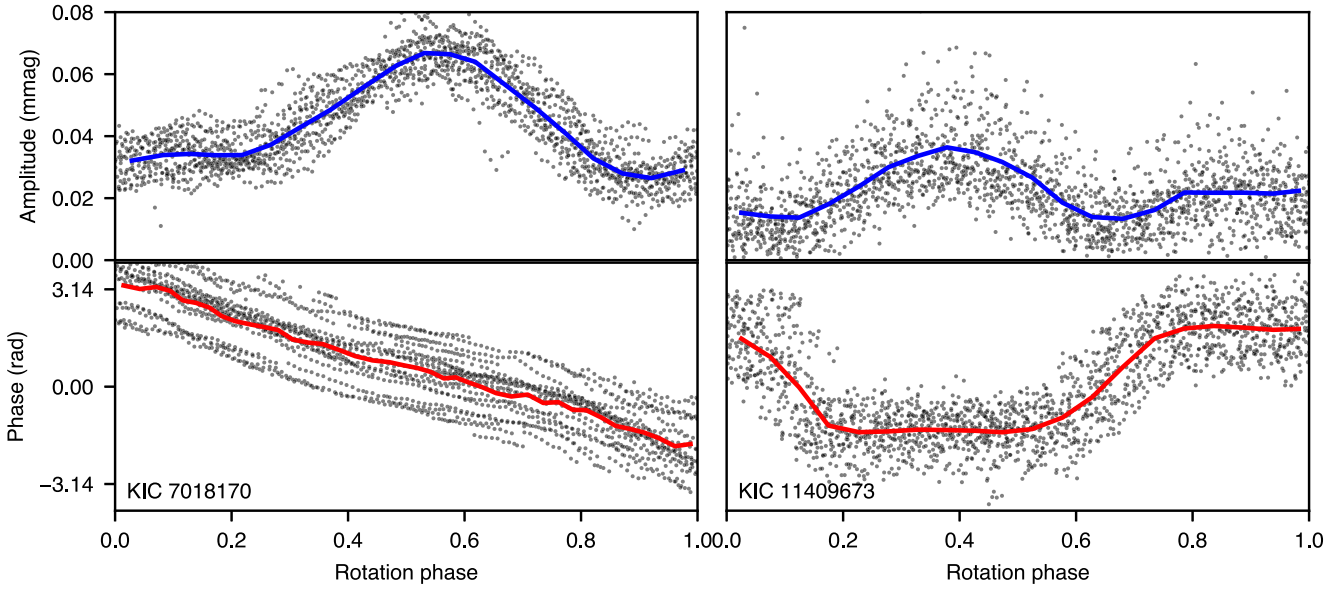

Figure 13. Amplitude and phase variations of KIC 7018170 (left) and KIC 11409673 (right). The top panels show the folded amplitude variations on the rotation period, whereas the bottom panels show the folded phase variations. The pulsation amplitude coincides with the rotational light extremum. A π rad phase change is observed when the line of sight passes over pulsation nodes. For KIC 7018170, the phase change occurs at a rotational phase of 0. The solid lines mark the binned data for clarity.

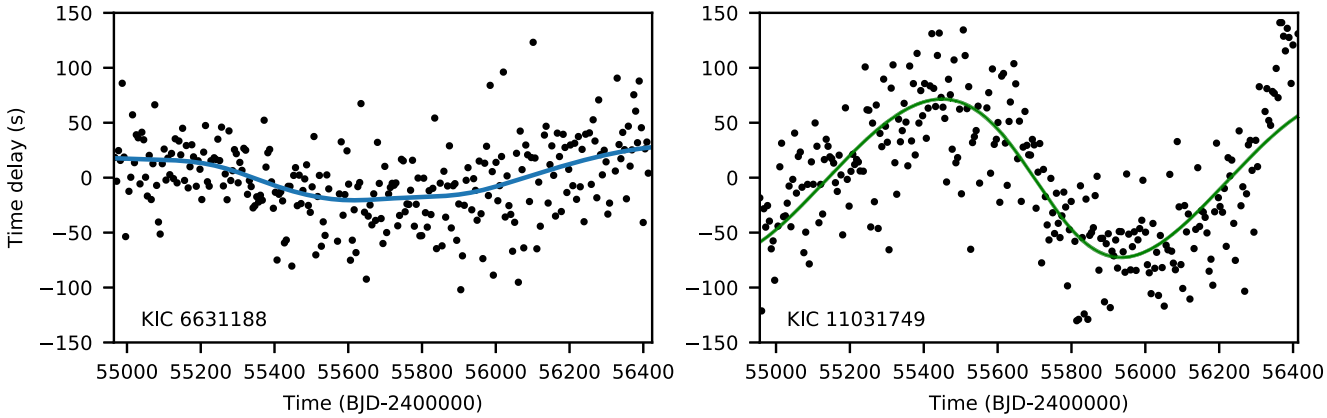

Figure 14. Left-hand panel: Observed time delay for KIC 6631188. The time delay, τ, is defined such that it is negative when the pulsating star is nearer to us than the barycentre of the system. The blue line is not an orbital solution fit, but rather the time delay as obtained by binning the signal for clarity. If the observed signal is truly periodic, it appears to be on a time-scale longer than the LC data. Right-hand panel: Observed time delays (black dots) and the fitted model (green line) for KIC 11031749. The phase modulation suggests a binary system of low eccentricity, whose orbital period is comparable to or longer than the time-base of the LC photometry.

Table 8. Model parameters of the non-adiabatic calculations. Shown are the surface helium abundance $Y_{\rm surf}$, minimum optical depth $\tau_{\rm min}$, and outer boundary condition in the pulsation code.

Model	$Y_{\rm surf}$	$\tau_{\rm min}$	Boundary condition
1	0.01	3.5×10^{-5}	Reflective
2	0.1	3.5×10^{-5}	Reflective
3	0.01	3.5×10^{-4}	Reflective
4	0.01	3.5×10^{-5}	Transmissive

(Section 4). Regardless, it makes for a useful test case for confirming modulation of its primary frequency. The amplitude spectrum of the modulation signal in Fig. 11 has a curious peak at twice the rotational frequency, 4.60 μHz, corresponding to a period of 2.52 d. This result implies that the spots are not necessarily aligned along the magnetic and pulsation axes, as was shown to be possible by Kochukhov et al. (2004).

The analysis of KIC 7018170 greatly benefits from amplitude modulation of its modes, as the PDCSAP flux pipeline removes any low-frequency content in the light curve. The modulation is calculated for all three modes present in the LC data, with the amplitude spectrum taken on the weighted average signal, which is thus dominated by ν_1. The frequency components of each mode multiplet are in phase, in good agreement with the oblique pulsator model. Indeed, it is quite remarkable that the secondary modes (ν_2, ν_3) in KIC 7018170 exhibit such clear amplitude modulation despite being of low SNR (Fig. 12). The amplitude spectrum of the variation in the signal is found to peak at 0.160 μHz agreeing with the rotation frequency identified from sidelobe splitting.

Table 9. Orbital parameters of KIC 11031749 obtained through phase modulation. ϖ is the angle from the nodal point to the periapsis, i is the inclination angle. a is the semimajor axis, e is the eccentricity, and ϕ_p is the phase of periastron.

Quantity	Value	Units
P_{orb}	1035.5 ± 0.5	d
$(a_1 \sin i)/c$	68.86 ± 0.13	s
e	0.203 ± 0.004	
ϕ_p	0.80 ± 0.03	
ϖ	0.08 ± 0.01	rad
$f(m_1, m_2, \sin i)$	0.000 327	$M_\odot$
$M_2 \sin i$	0.105 ± 0.001	$M_\odot$

No evidence of amplitude modulation can be found in KIC 11031749. We can however speculate on the nature of the lack of amplitude modulation and attribute it to two possibilities; either the position of the pulsation pole does not move relative to the observer, or the rotation period is much longer than the 4-yr *Kepler* data. Thus, no rotation period can be ascribed based on modulation of the principal frequency. KIC 11296437 shows a periodic signal in its amplitude modulation corresponding to the rotational period for only the high-frequency (ν_1) mode, with a frequency of 1.63 μHz. The low-frequency modes (ν_2, ν_3) show no evidence of amplitude modulation, suggesting that they could possibly belong to an orbital companion. KIC 11409673 has a clear low-frequency signal and harmonic present in the light curve beginning at 0.940 μHz. Amplitude modulation of its primary oscillation frequency shows evidence of rotation in good agreement with the low-frequency signal. The peak in the amplitude spectrum of the modulation confirms the rotation period of 12.310 d derived in Section 4.

Fig. 13 shows the variation of the pulsation amplitude and phase over the rotation period of the two stars in this work found to have observable phase crossings, KIC 7018170 and KIC 11409673. The maximum amplitude coincides with light maximum, which is expected when the spots producing the light variations are closely aligned with the magnetic and pulsation poles. The amplitude does not reach zero in KIC 7018170, but almost does in KIC 11409673. Since the amplitude does not go to zero for KIC 7018170, we can see that the mode is distorted.

5.5 Phase modulation from binarity

Both KIC 6631188 and KIC 11031749 show long-term phase variations independent of their rotation. If the frequency variability of KIC 11031749 is modelled as modulation of its phase due to binary reflex motion from an orbital companion, its orbital properties can be derived following the phase modulation technique (Murphy et al. 2014). To examine this, the light curve was separated into 5-d segments, where the phase of each segment at the primary frequency was calculated through a discrete Fourier transform. We then converted the phases into light arrival times (τ) by dividing by the frequency, from which a map of the binary orbit was constructed. A Hamiltonian Markov Chain Monte Carlo sampler was then applied to fit the time delay curve through the use of PyMC3 (Salvatier, Wiecki & Fonnesbeck 2016). The sampler was run simultaneously over 4 chains for 5000 draws each, with 2000 tuning steps. The resulting fit is shown in Fig. 14, with extracted orbital parameters in Table 9. These parameters give a binary mass function $f(m_1, m_2, \sin i) = 0.000\,327\ M_\odot$. Assuming a primary mass M_1 from Table 1 of 1.78 $M_\odot$, we obtain a lower limit on the mass of the companion to be 0.105 $M_\odot$, placing its potential companion as a low-mass M-dwarf.

KIC 6631188 also shows signs of frequency modulation (Fig. 14). However, if this modulation is truly from a stellar companion then its orbital period must be much longer than the time base of the *Kepler* data. The PM method can only be used when at least one full binary orbit is observed in the time delay curve. Thus, no orbital solution can be presented here.

It is important to note the scarcity of Ap stars in binary systems. Indeed, the much smaller subset of roAp stars have a low chance of being found in a binary (Abt & Snowden 1973; North et al. 1998; Folsom et al. 2014); however, few techniques can adequately observe the low-mass companion presented here. Although frequency modulation in roAp stars has been inferred in the past to be a consequence of binary motion, two out of the six stars presented in this work show evidence of coherent frequency/phase modulation. Whether this modulation is a consequence of changes in the pulsation cavity, magnetic field, or externally caused by orbital perturbations of a companion remains to be seen, and requires spectroscopic follow-up to rule out orbital motion via a radial velocity analysis.

6 CONCLUSIONS

We presented the results of a search for rapid oscillators in the *Kepler* LC data using super-Nyquist asteroseismology to reliably distinguish between real and aliased pulsation frequencies. We selected over 69 000 stars whose temperatures lie within the known range of roAp stars, and based on a search for high-frequency non-alias pulsations, have detected unambiguous oscillations in six stars – KIC 6631188, KIC 7018170, KIC 10685175, KIC 11031749, KIC 11296437, and KIC 11409673. LAMOST or Keck spectra of five of these stars shows that they exhibit unusual abundances of rare Earth elements, the signature of an Ap star, with the final target , KIC 10685175, already being confirmed as chemically peculiar in the literature.

This research marks a significant step in our search for roAp stars, and indeed, all high-frequency pulsators. To the best of our knowledge, this is the first time super-Nyquist asteroseismology has been used solely for identification of oscillation modes to such a high frequency. Although we expect many new roAp stars to be found in the *TESS* Data Releases, *Kepler* had the advantage of being able to observe stars of much fainter magnitude for a longer time-span, revealing pulsations of lower amplitude.

ACKNOWLEDGEMENTS

We are thankful to the entire *Kepler* team for such incredible data. DRH gratefully acknowledges the support of the Australian Government Research Training Program (AGRTP) and University of Sydney Merit Award scholarships. This research has been supported by the Australian Government through the Australian Research Council DECRA grant number DE180101104. DLH and DWK acknowledge financial support from the Science and Technology Facilities Council (STFC) via grant ST/M000877/1. MC is supported in the form of work contract funded by national funds through Fundação para a Ciência e Tecnologia (FCT) and acknowledges the supported by FCT through national funds and by FEDER through COMPETE2020 by these grants: UID/FIS/04434/2019, PTDC/FIS-AST/30389/2017 and POCI-01-0145-FEDER-030389. DH acknowledges support by the National Science Foundation (AST-1717000).

This work has made use of data from the European Space Agency (ESA) mission *Gaia* (https://www.cosmos.esa.int/gaia), processed by the *Gaia* Data Processing and Analysis Consortium (DPAC, https://www.cosmos.esa.int/web/gaia/dpac/consortium). Funding for the DPAC has been provided by national institutions, in particular the institutions participating in the *Gaia* Multilateral Agreement.

The authors wish to recognize and acknowledge the very significant cultural role and reverence that the summit of Maunakea has always had within the indigenous Hawai'ian community. We are most fortunate to have the opportunity to conduct observations from this mountain. This research was partially conducted during the Exostar19 program at the Kavli Institute for Theoretical Physics at UC Santa Barbara, which was supported in part by the National Science Foundation under Grant No. NSF PHY-1748958.

Guoshoujing Telescope (the Large Sky Area Multi-Object Fiber Spectroscopic Telescope; LAMOST) is a National Major Scientific Project built by the Chinese Academy of Sciences. Funding for the project has been provided by the National Development and Reform Commission. LAMOST is operated and managed by the National Astronomical Observatories, Chinese Academy of Sciences.

REFERENCES

Abt H. A., Morrell N. I., 1995, ApJS, 99, 135
Abt H. A., Snowden M. S., 1973, ApJS, 25, 137
Bailer-Jones C. A. L., Rybizki J., Fouesneau M., Mantelet G., Andrae R., 2018, AJ, 156, 58
Balmforth N. J., Cunha M. S., Dolez N., Gough D. O., Vauclair S., 2001, MNRAS, 323, 362
Balona L. A. et al., 2011a, MNRAS, 410, 517
Balona L. A. et al., 2011b, MNRAS, 413, 2651
Balona L. A. et al., 2013, MNRAS, 432, 2808
Balona L. A., Holdsworth D. L., Cunha M. S., 2019, MNRAS, 487, 2117
Bell K. J., Hermes J. J., Vanderbosch Z., Montgomery M. H., Winget D. E., Dennihy E., Fuchs J. T., Tremblay P.-E., 2017, ApJ, 851, 24
Bigot L., Dziembowski W. A., 2003, Ap&SS, 284, 217
Bigot L., Kurtz D. W., 2011, A&A, 536, A73
Borucki W. J. et al., 2010, Science, 327, 977
Carnall A. C., 2017, preprint (arXiv:1705.05165)
Chaplin W. J., Elsworth Y., Davies G. R., Campante T. L., Handberg R., Miglio A., Basu S., 2014, MNRAS, 445, 946
Cunha M. S. et al., 2019, MNRAS, 487, 3
Cunha M. S., 2002, MNRAS, 333, 47
Cunha M. S., Alentiev D., Brandão I. M., Perraut K., 2013, MNRAS, 436, 1639
Dotter A., 2016, ApJS, 222, 8
Drury J. A. et al., 2017, MNRAS, 471, 3193
Dziembowski W., Goode P. R., 1985, ApJ, 296, L27
Folsom C. P., Wade G. A., Likuski K., Kochukhov O., Alecian E., Shulyak D., Johnson N. M., 2014, Proc. IAU Symp., Vol. 302. Magnetic Fields Throughout Stellar Evolution. Kluwer, Dordrecht, p. 313
Green G., 2018, J. Open Source Softw., 3, 695
Green G. M. et al., 2018, MNRAS, 478, 651
Hartmann M., Hatzes A. P., 2015, A&A, 582, A84
Hekker S., Christensen-Dalsgaard J., 2017, A&AR, 25, 1
Holdsworth D. L. et al., 2014a, MNRAS, 439, 2078
Holdsworth D. L., Smalley B., Kurtz D. W., Southworth J., Cunha M. S., Clubb K. I., 2014b, MNRAS, 443, 2049
Holdsworth D. L., Kurtz D. W., Smalley B., Saio H., Handler G., Murphy S. J., Lehmann H., 2016, MNRAS, 462, 876
Holdsworth D. L., Cunha M. S., Shibahashi H., Kurtz D. W., Bowman D. M., 2018a, MNRAS, 480, 2976
Holdsworth D. L., Saio H., Sefako R. R., Bowman D. M., 2018b, MNRAS, 480, 2405
Howard A. W. et al., 2010, ApJ, 721, 1467
Huber D. et al., 2011, ApJ, 743, 143
Huber D. et al., 2017, ApJ, 844, 102
Hümmerich S. et al., 2018, A&A, 619, A98
Jiménez A., García R. A., Pallé P. L., 2011, ApJ, 743, 99
Joshi S. et al., 2016, A&A, 590, A116
Joshi S., 2005, J. Astrophys. Astron., 26, 193
Kirk B. et al., 2016, AJ, 151, 68
Kochukhov O., 2009, Commun. Asteroseismol., 159, 61
Kochukhov O., Drake N. A., Piskunov N., de la Reza R., 2004, A&A, 424, 935
Kurtz D. W., 1990, ARA&A, 28, 607
Kurtz D. W. et al., 2011, MNRAS, 414, 3
Kurtz D. W., 1978, Inf. Bull. Var. Stars, 1436, 1
Kurtz D. W., 1982, MNRAS, 200, 807
Kurtz D. W., 1985, MNRAS, 213, 773
Kurtz D. W., 2000, Variable Stars as Essential Astrophysical Tools. Springer Netherlands, Dordrecht, p. 313
Landstreet J. D., Mathys G., 2000, A&A, 359, 213
Martinez P., Kurtz D. W., Kauffmann G. M., 1991, MNRAS, 250, 666
Mathur S., García R. A., Huber D., Regulo C., Stello D., Beck P. G., Houmani K., Salabert D., 2016, ApJ, 827, 50
Mathur S. et al., 2017, ApJS, 229, 30
Mathys G., 2015, IAU General Assembly, 22, 2256010
Mathys G., 2017, A&A, 601, A14
Matthews J. M., Kurtz D. W., Martinez P., 1999, ApJ, 511, 422
Morgan W. W., 1933, ApJ, 77, 330
Murphy S. J., 2015a, PhD thesis, Springer International Publishing
Murphy S. J., 2015b, in Murphy S. J., ed., Springer Thesis, Investigating the A-Type Stars Using Kepler Data. Springer International Publishing, Cham, p. 53
Murphy S. J., 2015c, MNRAS, 453, 2569
Murphy S. J., Shibahashi H., Kurtz D. W., 2013, MNRAS, 430, 2986
Murphy S. J., Bedding T. R., Shibahashi H., Kurtz D. W., Kjeldsen H., 2014, MNRAS, 441, 2515
Murphy S. J., Hey D., Van Reeth T., Bedding T. R., 2019, MNRAS, 485, 2380
North P., Ginestet N., Carquillat J.-M., Carrier F., Udry S., 1998, CAOSP, 27, 179
Paunzen E., Netopil M., Rode-Paunzen M., Handler G., Božić H., Ruždjak D., Sudar D., 2012, A&A, 542, A89
Pinsonneault M. H., An D., Molenda-Żakowicz J., Chaplin W. J., Metcalfe T. S., Bruntt H., 2012, ApJS, 199, 30
Reinhold T., Gizon L., 2015, A&A, 583, A65
Reinhold T., Reiners A., Basri G., 2013, A&A, 560, A4
Ricker G. R. et al., 2014, J. Astron. Telesc. Instrum. Syst., 1, 014003
Royer F., 2009, in Rozelot J.-P., Neiner C., eds, Lecture Notes in Physics, The Rotation of Sun and Stars. Springer, Berlin, Heidelberg, p. 207
Royer F., Zorec J., Gómez A. E., 2007, A&A, 463, 671
Ryabchikova T., Sachkov M., Kochukhov O., Lyashko D., 2007, A&A, 473, 907
Saio H., 2005, MNRAS, 360, 1022
Saio H., 2013, Proc. IAU Symp., 9. Precision Asteroseismology. Kluwer, Dordrecht, p. 197
Salvatier J., Wiecki T. V., Fonnesbeck C., 2016, PeerJ Comput. Sci., 2, e55
Sanders J. L., Das P., 2018, MNRAS, 481, 4093
Schöller M., Correia S., Hubrig S., Kurtz D. W., 2012, A&A, 545, A38
Shibahashi H., Murphy S. J., 2018, preprint (arXiv:1811.10205)
Shibahashi H., Saio H., 1985a, PASJ, 37, 245
Shibahashi H., Saio H., 1985b, PASJ, 37, 601
Shibahashi H., Takata M., 1993, ASP Conf. Ser., IAU Colloq. 137: Inside the Stars. Astron. Soc. Pac., San Francisco, p. 563
Shporer A. et al., 2016, ApJ, 829, 34
Smalley B. et al., 2015, MNRAS, 452, 3334
Sousa S. G., Cunha M. S., 2008, MNRAS, 386, 531
Stumpe M. C., Smith J. C., Catanzarite J. H., Cleve J. E. V., Jenkins J. M., Twicken J. D., Girouard F. R., 2014, PASP, 126, 100
Takata M., Shibahashi H., 1994, PASJ, 46, 301
Takata M., Shibahashi H., 1995, PASJ, 47, 219

Torres G., 2010, AJ, 140, 1158
Vinícius Z., Barentsen G., Hedges C., Gully-Santiago M., Cody A. M., 2018, Lightkurve: Kepler and TESS time series analysis in Python. Astrophysics Source Code Library
Vogt S. S. et al., 1994, in Crawford D. L., Craine E. R., eds, Proc. SPIE Conf. Ser., Vol. 2198. Instrumentation in Astronomy VIII. SPIE, Bellingham, p. 362
Yu J., Huber D., Bedding T. R., Stello D., Murphy S. J., Xiang M., Bi S., Li T., 2016, MNRAS, 463, 1297
Zhao G., Zhao Y., Chu Y., Jing Y., Deng L., 2012, preprint (astro-ph/1206.3569)

APPENDIX A: LEAST-SQUARES FIT OF PULSATION MODES FOR KIC 11409673

We provide here the force-fitted sidelobes for the other sections of data in KIC 11409673.

Table A1. Force-fitted pulsations in KIC 11409673 for Sections 2–4. The zero-points were chosen to force the first set of sidelobes to be equal, and are BJD 2455501.39754, BJD 2455870.64075, and BJD 2456240.07652, respectively.

ID	Frequency (μHz)	Amplitude $_{\text{Intrinsic}}$ (mmag)	Phase (rad)
Section 2			
$\nu_1 - \nu_{\text{rot}}$	2499.992 03	0.303 ± 0.018	-2.239 ± 0.058
ν_1	2500.932 22	0.086 ± 0.018	-2.437 ± 0.206
$\nu_1 + \nu_{\text{rot}}$	2501.872 42	0.255 ± 0.018	-2.239 ± 0.069
Section 3			
$\nu_1 - \nu_{\text{rot}}$	2499.974 49	0.311 ± 0.017	-1.858 ± 0.056
ν_1	2500.914 69	0.090 ± 0.017	-1.787 ± 0.194
$\nu_1 + \nu_{\text{rot}}$	2501.854 89	0.221 ± 0.017	-1.858 ± 0.079
Section 4			
$\nu_1 - \nu_{\text{rot}}$	2499.963 84	0.281 ± 0.017	-2.169 ± 0.061
ν_1	2500.904 04	0.079 ± 0.017	-2.243 ± 0.217
$\nu_1 + \nu_{\text{rot}}$	2501.844 24	0.241 ± 0.017	-2.169 ± 0.071

This paper has been typeset from a TEX/LATEX file prepared by the author.